DESIGN AND DEVELOPMENT OF ROBOTIC SYSTEM FOR ENDOVASCULAR PROCEDURES

BY

NAVEEN KUMAR SANKARAN

THESIS

Submitted in partial fulfillment of the requirements
for the degree of Master of Science in Systems and Entrepreneurial Engineering
in the Graduate College of the
University of Illinois at Urbana-Champaign, 2016

Urbana, Illinois

Adviser:

Professor Thenkurussi Kesavadas

Abstract

Endovascular surgeries are highly preferred minimally invasive procedures performed through blood vessels for diagnostic and therapeutic purposes. In conventional open surgery, surgeons have complete control on the surgical tool, but in the case of endovascular procedures, a highly flexible tool, which is operated from distal end provides an indirect control. Moreover, the operating end of these flexible tools inside a patient are controlled from distal end, outside patient's body, with an imperceptible force feedback from the tool. Even though fluoroscopic images like X-rays provide a temporary solution, the perceptive of depth is not available in these visual feedback and the prolonged hazardous radiations do not provide a safer working environment for surgeons. A tele-operated robotic systems have enhanced the surgical conditions nevertheless, it decline to provide a better system which can help surgeons to use their intuitive surgical skills. Additionally, these robotic system requires replacement of the low cost conventional surgical tools with expensive one, thus increasing the procedural cost. This thesis work addresses these two issues in the endovascular robotic systems by 1. Developing an intuitive user interface console to help ease of transfer of surgical skills for surgeons, 2. Developing an in-built force feedback sensing mechanism in the robot that is adaptable to conventional surgical tool. A new interventional robotic system (IRS) with teleoperation control was developed to isolating the surgeons from hazardous radiation. The master console of IRS is design to capture surgeon's conventional surgical gestures thus, eliminating the need for learning new skills to manipulate surgical robots. IRS ensures patient's safety by providing haptic feedback to surgeons using reactive force experienced by surgical tool. IRS also has the adaptability to use the conventional surgical tool of wide range of dimensions. Finally, the force measurement evaluation and performance assessment of the IRS were presented. The future scopes of this research work are briefly discussed.

To my brother Akshaya kumar, my parents & family,
for their love & support.

Acknowledgments

I would like to gratefully acknowledge the advice, help and guidance that I have received to successfully complete this thesis. First, I express my deepest gratitude to my adviser, Professor Thenkurussi Kesavadas for his inspiration, guidance, encouragement and support.

I am extremely thankful to Department of Industrial and Enterprise Systems Engineering, University of Illinois at Urbana-Champaign for their constructive curriculum. I also thank the Professor Rakesh Nagi, and Associate Professor R. S. Sreenivas for their support throughout my graduate program.

A special thanks to Dr. Adnan Siddiqui, MD and Dr. Kenneth Snyder, MD, of Department of Neurosurgery, University at Buffalo for their feedback and advice on interventional surgical procedures which had been influential and essential throughout this research work.

I would certainly be remiss not to mention and sincerely thank the members of Health Care Engineering Systems Center who provided invaluable research and academic assistance throughout my graduate studies. This include Dr. Antonios Michalos, Dr. Pramod Chembrammel, Xiao Li, Yao Li, Kuocheng Wang and Shrey Pareek.

I would also acknowledge the support of Health Care Engineering Systems Center of University of Illinois at Urbana-Champaign, State University of New York at Buffalo, The Jacobs Institute in Buffalo.

TABLE OF CONTENTS

List of Figures

CHAPTER 1

Introduction

Over the last decade medical robotic systems have revolutionized the surgical procedures. Invasive open surgeries are reduced to minimally invasive procedures. As a result, numerous challenges including duration, patient recovery, blood loss, precision, hand tremor, visibility, hazardous radiations, etc. are greatly improved. Minimally invasive surgical procedures are often preferred to open surgical procedures due to their minimal recovery time, less discomfort to patient and less damage to healthy tissues. This chapter provides an overview of minimally invasive surgery and a detail description of endovascular surgery. This is followed by discussion of challenges involved in endovascular surgery and the motivation of this research work.

1.1 Minimally Invasive Surgery

Surgical procedures performed with minimal incisions to accomplish a task are commonly referred to as minimally invasive surgeries (MIS). Many medical procedures such as endovascular, laparoscopic, endoscopy, arthroscopy, microsurgery, keyhole, etc fall into this division. Due to small incision size, direct view of the surgical area is limited to surgeons. To achieve visual feedback, imaging systems such as endoscopes or radiological devices such as X-Rays, MRI, CT-scan (as shown in Fig. 1.1) etc. are used.

To access the surgical area to perform procedure with high precision dexterous tools were developed which have been manipulated directly by surgeons or indirectly with the help of robots. Several robotic devices have assisted various surgical procedures: PUMA 560 robotics surgical arm[25] was used to perform neurosurgical biopsy, ROBODOC[26] in hip-replacement surgery, da Vinci Surgical System [27] perform laparoscopic surgery. This list includes other systems (as shown in Fig. 1.2) like Zeus [28], Makoplasty [29],

Figure 1.1: Imaging devices (a. Magnetic resonance imaging (image courtesy [1]), b. Computed tomography (image courtesy [2]), c. X-ray (image courtesy [3]))

NeuroArm [30], CorPath 200 robotic system [31], Magellan Robotic System [32], etc. This rapid development of technology has enabled advancement in surgical procedures with new techniques to diagnose, monitor and treat.

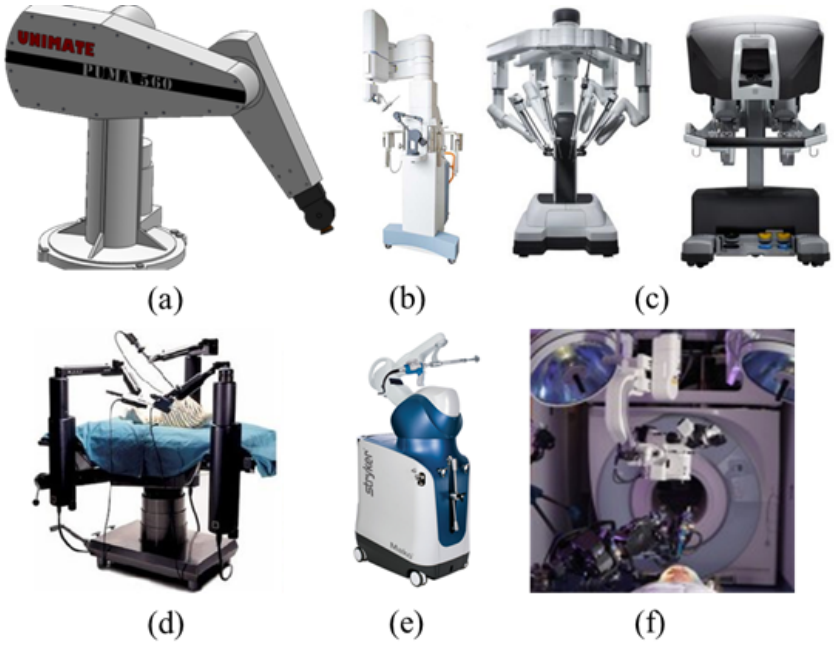

Figure 1.2: Medical robotics system (a. PUMA 560 (image courtesy [4]), b. ROBODOC (image courtesy [5]), c. da Vinci Surgical System (image courtesy [6]), d. Zeus (image courtesy [7]), e. Makoplasty (image courtesy [8]), f. NeuroArm (image courtesy [9]))

1.2 Endovascular Surgery

Medical procedures performed by navigating blood circulatory system are commonly referred to as endovascular surgery. Endovascular surgery also called interventional surgery, are minimally invasive procedures that are performed for diagnostic and therapeutic purposes with the help of imaging systems. Various physicians in internal medicine, surgery and radiology perform the endovascular surgery procedures. Specialists like cardiologists, neurologists and nephrologists are specialized to identify and treat abnormalities of internal organs and blood vessels. According to the statistics report [33] in 2008, approximately 3.6 million interventional procedures were performed and it was expected to increase at a compound annual rate of 3.7%. The number of patients preferring this procedure is also increasing rapidly because of advantages like reduced pain, blood loss, scars and recovery time. Procedures performed near heart or on coronary arteries are called percutaneous coronary interventions (PCI) [34]. Procedures performed on blood vessels near neck and brain are called neuro-interventional surgery. The endovascular procedures are used for diagnosing abnormality conditions like blood clots, plaque, aneurysms, stenosis etc as shown in Fig. 1.3.

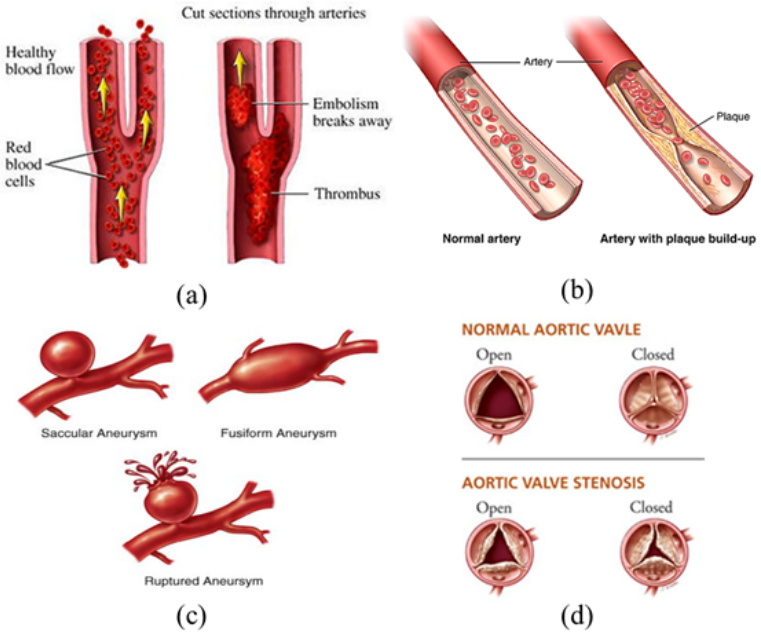

Figure 1.3: Endovascular abnormality (a. Blood clots (image courtesy [10]), b. Plaque (image courtesy [11]), c. Aneurysms (image courtesy [12]), d. Stenosis (image courtesy [13]))

Treatment options for the blood clot and plaque abnormalities are called thrombectomy. In thrombectomy procedures, the blood clot is accessed via blood vessels and are removed either using a suction device or a mechanical device as shown in Fig. 1.4(a). Treatment options for aneurysms (weakening of artery) and stenosis (narrowing of artery) are commonly referred as angioplasty. In this procedure, the arterial vessels are strengthened or reconstructed using balloons or vessel scaffolding devices called stents as shown in Fig. 1.4(b).

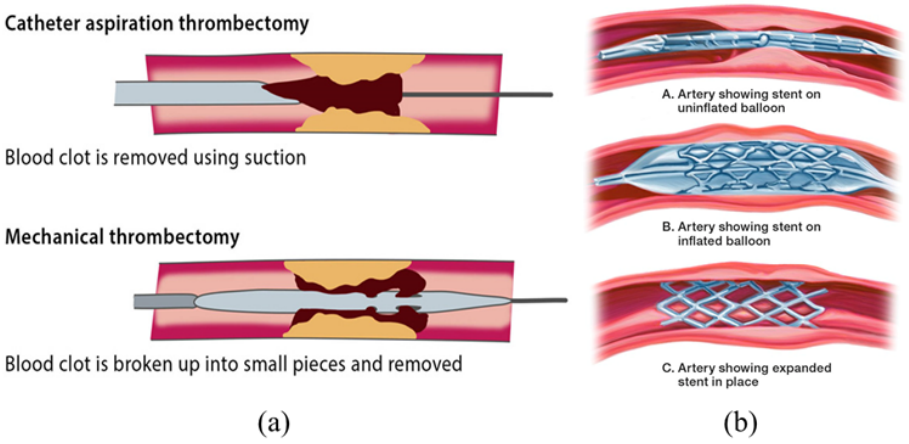

Figure 1.4: (a)Thrombectomy: mechanical and suction methods (image courtesy [14]), (b)Angioplasty: balloon stenting (image courtesy [15])

An endovascular procedure commonly begins with cannulation, in which an incision is made on the blood vessel. Most common insertion sites are on the femoral artery, brachial artery and radial artery which are respectively in the groin, arm and wrist regions as shown in Fig. 1.5. After this, a highly flexible surgical tools such as guidewires or catheters (henceforth referred as tools) are inserted into the body.

Navigation inside vasculature requires three components: path to navigate, current position and orientation of the tools and safe navigation without damaging tissues. To visualize the path for navigation, the anatomy of vasculature is obtained by injecting a radioactive contrast dye inside the blood stream which is visible using imaging devices like X-rays, CT scan, etc. The flow of fluoroscopic dye can also be recorded for detailed study after procedure. The surgical tools used are themselves visible in the fluoroscopic images which provide approximate estimation of position and orientation of the tool inside the vasculature. In addition to visual feedback from the

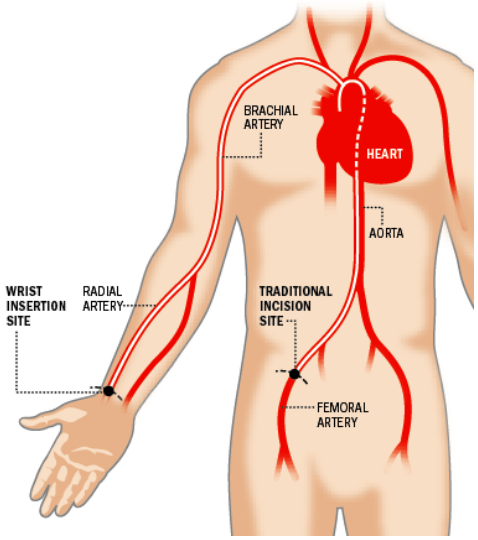

Figure 1.5: Surgical insertion sites (image courtesy [16])

imaging devices, surgeons depend on force feedback via surgical tool for safe navigation. The forces experienced by the tool from interaction with the walls of vasculature and from obstacles are thus crucial parameters.

Guidewire as shown in Fig. 1.6 are flexible wire and catheters as shown in Fig. 1.7 are hollows tubes which are used in pair sliding over each other to navigate the vasculature. Guidewires apart from the navigation purpose are also essential for tool exchanges which is required since the arteries' cross section varies in different parts of anatomy and surgeons use different size of tools during a procedure. The guidewires are classified based on various parameter like tip load capacity, stiffness, outer covering, tip type etc.

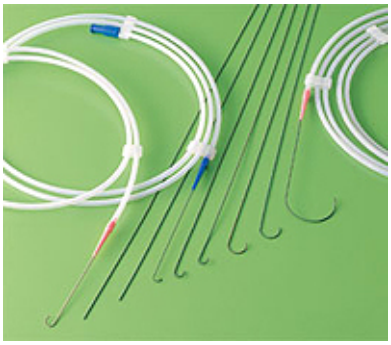

Figure 1.6: Different guidewire shapes (image courtesy [17])

Catheters are classified based on tip or head shapes. Annular structure of catheter also acts as a delivery system to inject radioactive contrast dye inside

blood vessel. This radioactive contrast dye provides visibility of vasculatures under fluoroscopic imaging devices. The diameter of these tools ranges from 3F (French scale: 3F=1mm) to 34F. There are specialized tools with features like balloons, stents etc. designed to meet the needs of surgeons.

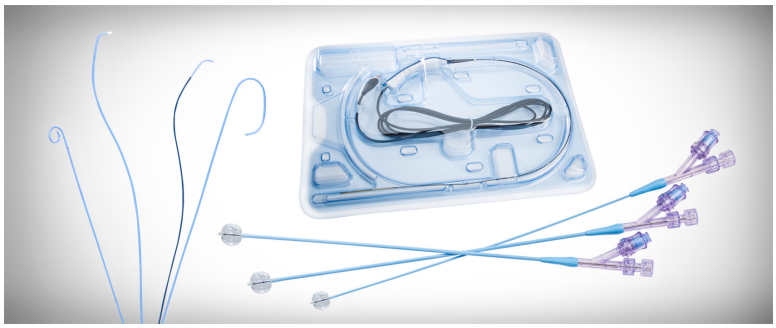

Figure 1.7: Different catheters types (image courtesy [18])

In addition to these conventional tools, advanced active tools are also developed with built-in sensors and can be remotely controlled. These active catheters as shown in Fig. 1.8 have reorientable tip which aids in navigation. A sensor at the tip measures the contact force between the tool and the tissues. There are various sensing methods adopted in these tools like micro force sensor, fiber-optics pressure sensor, strain gauges etc. The actuators with belt driven mechanism deflects the tip of the tool in the desired direction. This deflection action is used to choose the direction of movement of the tool.

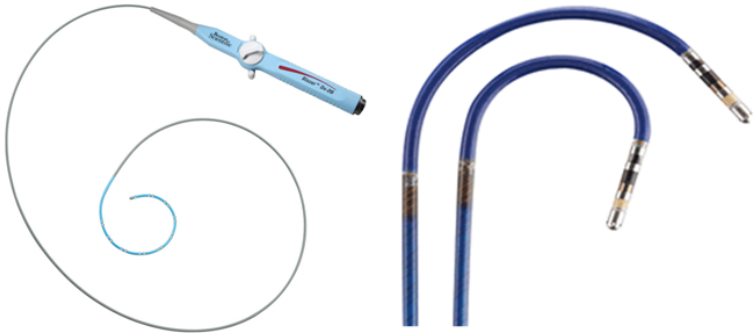

Figure 1.8: Active tip catheter (image courtesy left [19] right [20])

Navigating the tools involves two actions: translation and rotational as shown in Fig. 1.9. The translation action performed on the tool will advance or retrieve the tool with in the vasculature. This translation motion is

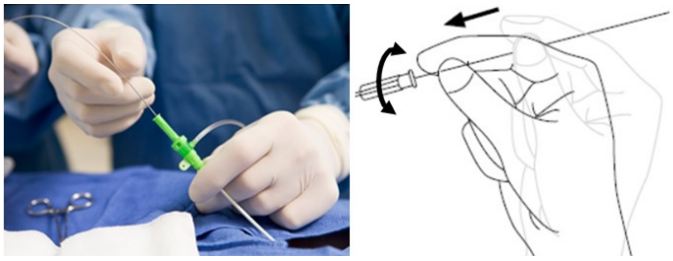

Figure 1.9: Tool manipulation (image courtesy left [21] right [22])

achieved by surgeon by push and pull actions on the surgical tool. The rotational actions are performed to steer the surgical tool to the correct branch of a bifurcation in vasculature. This rotational motion is achieved by twisting or torqueing action on the tool in the desired direction. For the rotational motion of the guidewire, conventionally surgeons use a torquer device as shown in Fig. 1.10 which is clutched to the guidewire. The torquer provides more grip to perform the rotational action on the guidewire.

Figure 1.10: Torquer (image courtesy [23])

During the procedure, the surgeon's hand feels resistance from the tool. This reactive force has three components: applied force(force applied by user on the tool), resistive force (force between the tool tip and vasculature structure) and frictional force (force between the vasculature and the entire length of tool inside patient). Figure 1.11 shows the example of steering performed inside the vasculature to navigate a lesion and branching in the vasculature.

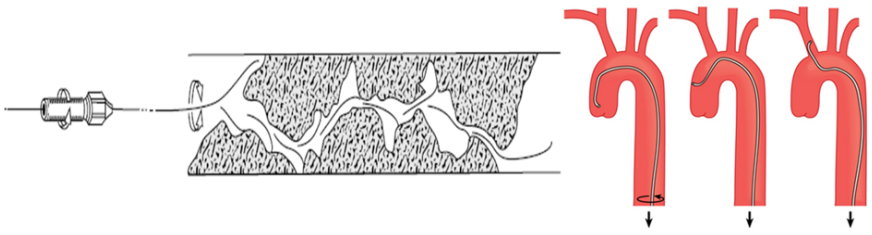

Figure 1.11: Steering of guidewire (image courtesy left [22] right [24])

1.3 Motivation

Triaging the issues in health care systems and improving the conditions are essential, to ensure patient's safety and better working ambiance. Endovascular procedures are intricate, since mistakes during a procedure could rupture the blood vessel, complicating patient's condition or even resulting in fatalities. The following are few challenges identified in the endovascular procedures.

- Potential occupational hazard to surgeons due to X radiations exposure from imaging devices.
- Highly flexible surgical tool has unpredictable dynamics of motion which makes precise steering difficult.
- Tortuous vasculature nature in human anatomy complicates simple procedure.
- Limited work volume and unknown tissue property demands precise hand movement for performing procedure.
- Tool manipulation is complicated since hand tremors could get amplified at the distal ends.
- Motor skills required to perform precise procedure requires extensive training.
- Imperceptible force feedback can result in administering unintended force.
- Active catheters are available only for a limited range of cross sectional dimensions making it unusable for smaller vasculature.
- Active catheters are expensive and thus increases the procedural cost.
- Error due to deviation of changing of intuitive skill between a manual procedure and a robot assisted procedure.
- User interface control of robotic systems deviates from the conventional manual tool handling skills.

- Limited visibility to the site of operation and the available visual feedback are only 2D images or reconstructed 3D images.

Although a few of these issues have been solved in the current robotics systems, there are still exist issues which require attention. The existing robotic systems decline to provide a better solution which will help surgeons to transfer their experience and intuitive surgical skills. In this thesis work, the design and development of an Interventional Robotic System (IRS) for the surgeons to perform the endovascular procedures with conventional hand actions providing real-time haptic feedback using passive surgical tools is discussed. The IRS augments the actions of surgeon unlike the existing devices. Using the same tools, the surgeon can perform the same surgical actions (translations and rotations) which will be captured by a sensing unit. These captured actions are used to command a robot unit to navigate the tool inside the vasculature. Although the control scheme is same as the master-slave scheme employed in the existing devices, the device lets the surgeon to perform the procedure in the same way as they perform in the conventional way using the tools. As a result, surgeons does not have to learn new skills to use the IRS and can use the procedural skills that they have acquired by experience from conventional procedures. The main advantages of our approach are: 1. no new skills have to be learned by surgeons, 2. eliminates the use of active surgical tools, 3. facilitates tele-operation, 4. uninterrupted continuous control, 5. passive reactive force sensing, 6. haptic feedback, 7. easiness to assemble and disassemble for sterilization.

CHAPTER 2

Literature Review

Numerous robotic systems have been developed by many companies and research groups around the world. These are in various stages of studies with phantom, animals and clinical trials. Robotic systems which are under in clinical trials [35][36][37] have demonstrated notable advantages which include reduced fluoroscopy content, lesser exposure to radiation for both patients and surgeons [38] and improved precision [39]. In spite of these advances, introduction of robots has deprived the surgeons from transferring their conventional and intuitive skills to perform procedures. One of the reasons for this has been the interfaces that the practitioners use to control the robot. Various control interfaces used are keypad, joystick, mouse, trackball, touch screens and robotic manipulators. Use of these interfaces deviates from the way surgeons performed conventionally. As a result, the interventional practitioners need to learn a new set of skills to use the robotic devices for interventional procedures. In this chapter, the existing robotic systems developed by companies and researchers are briefly discussed focusing on system design, user interface and haptic feedback.

2.1 Commercial Robotic Systems

Some of the currently available commercial systems are Amigo™ remote catheter system [40], CorPath® 200 robotic system [31], Magellan™ Robotic System [32] and Stereotaxis Epoch® [41]. These systems are in various stages of healthcare implementations. All these systems commonly consist of slave robot mounted closer to the patient and a master console remotely located for teleoperation. The surgeons perform the navigation action by commanding from the master console. The actions of the surgeons at the console are guided by X-ray fluoroscopic images available at the console. Each of the

existing devices are discussed in detail as follows.

Amigo™ remote catheter system [40] [36], uses an ablation catheter which is manipulated by the robot arm and is controlled using a wired hand held controller. The slave manipulator consists of a turret and sled assembly with a docking station to mount the surgical tool. The translation motion of the ablation catheter is achieved with the button control on the catheter handle and the rotary motion is achieved by knob control which rotation of turret on sled assembly thus rotating the catheter. The hand held controller has 4 control elements. They are (1) rotation, (2) catheter tip deflection, and (3) advance and withdraw buttons. The inset shows the infrared safety beam on the opposite side of the handle (4) that prevents inadvertent catheter movement.

CorPath® 200 robotic system [31] [37], uses a guidewire and a balloon/stent. These tools are mounted on a cassette which is placed on the slave manipulator. The robotic drive mechanism is coupled to the single use cassette, the translation motions are performed with friction rollers and rotational motion is performed with the rotational drive inside the cassette. The tools are remotely operated from the console using the joysticks or touch screen buttons. The joystick on the right side controls the guidewire's translation motion with lever action and rotation motion with of twist of the joystick. Similarly, the joystick on the left control the movement of the balloon/stent.

Magellan™ system [32] [42], uses a guidewire and an active catheter which are mounted on a robotic arm. The robotic manipulator has a friction roller mechanism for translation motion and a set of friction slider mechanism for rotation motion. Additionally, the active catheter has addition dexterity for navigation. The robotic arm is controlled by surgeon from a console unit with a selection panel, buttons and a robotic manipulator. The up and down arrow on the control panel is used to control the translation motion of the catheter. The course of movements are altered with multiple options like buttons, knob, and 3D manipulator. A set of buttons rotate the guidewire, another set of button is used to deflect the active catheter, knob is used to achieve axial rotation of the catheter and the 3D manipulator is also used to rotate the active catheter. The catheter contact force is measured and communicated to the operator as haptic feedback.

Stereotaxis Epoch® [41] [43] [44], uses a custom built magnetic guidewire and catheter which are oriented and steered in permanent magnetic field,

and a mechanical drive is used to advance the tool. The tip orientation and linear position control are achieved using a coordinated action of joystick, the roller wheels and mouse control [45].

2.2 Researchers' Robotic Systems

Researchers across the world have contributed numerous work in progressing towards refining technology for interventional procedures. In this section, robotic systems developed by researchers are reviewed to discuss the system design, the user interface and the force measurement. Systems design focuses on the actuation mechanism to achieve motion of the surgical tool, the user interface focuses on the control features provided to navigate the surgical tool and the force measurement discusses the different techniques of measurement.

2.2.1 System Design and User Interface

Zakaria et al [46] has developed a tele-operated catheter-guide system consisting a slave robot and a hand-held master controller. The manipulator has friction roller for linear motion and a gear assembly for rotary motion of catheter. The controller has an encoder as well as a pulse counter to detect the positional information of the control elements like translation and rotation.

Guo et al [47], developed a master-slave tele-operation system which captures surgeon's actions. The linear motion is achieved by a repositioning mechanism installed on a sliding platform and the rotatory motion is performed by assembly of grasper and belt driven mechanism. The surgeon's push and pull actions on the handle are sensed along with the applied force by the master manipulator.

Payne et al [48] developed an integrated unit in which the master and slave units are built as single unit. In this device, the surgeon's actions are captured using a master controller. The master controller is translated by the surgeon and the slave platform replicates this motion with the help of linear actuator. Positive feed of the catheter is achieved by repositioning the master and slave platforms using a clutch mechanism. The repositioning interrupts the actions of the surgeon which is contrary to the natural actions

in conventional procedure. This device did not have the option for teleoperation because of the integration of master and slave parts as single unit.

Arai et al [49], has built a system which drives the catheter with friction roller mechanism. The master controller of this system has a fulcrum based mechanism to capture the surgeon's hand motion directly.

Yang et al [50] developed a guidewire feeding robot for conventional guidewire. This system has three sets of fingers, fixed finger to guide the guidewire, promoting finger for translational motion and rotating finger for rotational motion. The promoting finger has pressure sensors which measures the resistive force.

Govindarajan et al [51], has developed a System for Endovascular Teleoperated Access (SETA) which has a friction roller mechanism for translation motion and a spring loaded gripper mechanism for rotation motion. The following are the list of components mark in figure 1, Pulley for travelling cart 2: Mounting arm 3: Travelling cart 4: Linear drive for guidewire 5: Linear drive for catheter 6: Steering stage for catheter 7: Entry point for guidewire, 8: Steering point for catheter and 9: Exit point of catheter into body.

Marcelli et al [52], developed a robotics system which operates with standard steerable electrophysiology catheter. The system facilitates translational and rotational motion along with the motions of the steerable catheter tip. The control commands are provided by means of joystick.

2.2.2 Force Measurement

Measuring the reactive force is crucial for the endovascular procedure as excessive force applied on the surgical tool can dislodge a plaque, rupture an aneurysm or the blood vessel itself. In conventional procedures, the reactive force felt by an experienced surgeon through the surgical tool aids them to judge the resistance offered by the vasculature. Considering the importance of this haptic feedback from the surgical tool many developers have adapted various ways to measure the forces encountered by the surgical tool. These force measurement techniques have been integrated with most of the robotic system to display the information to the user in real time. These techniques are capable of measuring either the distal forces or the proximal forces. The proximal forces are direct measurements of the contact forces between sur-

gical tool and vasculature, which is measured by means of special active catheters which are equipped with sensors at the tip of the devices. The distal forces are indirect measurement of contact forces which is measured closer to the region of actuation outside the human body by sensing devices like load cell or pressure sensor. The distal force data measured represent various components of forces like contact force between the surgical tool tip and the vasculature, resistive force between the entire surgical tool and the rest of the vasculature, the friction force at the contact surfaces of the robotic device and the surgical tool.

A few examples of distal force measurement techniques adopted by the researchers are as follows. Payne et al [48] has used strain measurement mounted on the conventional passive catheter tips. The deflection of the catheter in contact with the blood vessel walls introduces strain in the sensor which in turn is converted to force values. Yang et al [50] guidewire feeding robot which operates on conventional guidewire has a promoting finger with pressure sensors which measures the resistive force. Guo et al [47], master-slave tele-operation system used a load cell to measure the reactive force in the catheter.

Alternatively, the proximal force measurement techniques have also been explored by various researchers. The following are few example of implementation, Marcelli et al [52], in their robotic system uses an active catheter with a force sensor at the tip, to monitor the proximal forces on the catheter. Tanimoto et al [53] and Polygerinos et al [54] developed active sensing methods using micro-force sensor and fiber-optic pressure sensors respectively, which are installed at the tip of catheter.

2.3 Summary of Literature Review

In most of the robotic systems, the actuation mechanism adapted for translation motion were either linear actuator or friction wheel. In case of the linear actuator based mechanism, the advancing motion is constrained by the length of the actuator stem due to which the system has to reposition itself. This repositioning mechanism is capable of disrupting a continuous feeding of surgical tool. On the other hand, friction wheel mechanism eliminates the repositioning movement and can operate on a continuously. The

rotary motion is commonly achieved by a coupled action of gripping the surgical tool and rotating it axially. Even though the development of steerable catheter eliminates the need for such rotatory motion it is still debated as the cost of active catheter is approx $2500 [55]. Using a steerable catheter will increase the cost of the interventional procedure.

Mostly commonly used user interfaces are keypad, joystick, mouse, trackball, touch screens and robotic manipulators. Apart from these controls options, few researchers have also custom built user interfaces to provide intuitive experience with the user interface. Among these, interfaces built with repositioning mechanism have the same issues as discussed above in the system design summary.

The force measurement techniques integrated with robotic system to measure either the distal forces or the proximal forces is an essential feature. These proximal force measurement techniques using active catheters are limited to few procedures because, the diameter of the active catheters are larger in diameter than the vasculatures cross section making it inaccessible to all organs. On the other hand, the distal force measurement techniques to determine the reactive forces represent similar to reactive force as surgeons experience on their hand during manual procedure.

CHAPTER 3

Design and Methodology

The maneuverability of a passive surgical tool inside the vasculature has two degrees of freedom; translational and rotational motions as shown in Fig. 1.9. The surgeon's intention to navigate the tool are reflected in his actions to translate or rotate actions. Also, the surgeon's response to reaction force from obstacle (wall of the vessel or a plaque) and friction are essential for success of procedure. These forces along with visual feedback aids the surgeon to make necessary decisions in order to navigate the tool.

3.1 Design Requirements

The robotic system design requirements are formulated as follows

1. The system should facilitate tele-operation to avoid radiation from imaging devices.
2. The system should not demand surgeons to learn new skills to operate the user interface of the robotics system to perform the procedure.
3. The system should provide continuous drive for maneuvering the surgical without interrupted actions.
4. The system should be capable of measuring distal forces thereby eliminating the need for active catheter.
5. The system should provide haptic feedback to the surgeons to alert the measured reactive force beyond safe limit.
6. The system should operate with the passive surgical tool of wide range of dimensions and also eliminate the need of active surgical tools.
7. The system should be easy to assemble and sterilize.

3.2 Design and Development

The interventional robotic system is developed in two phases: the first phase of development focuses on conceptual verification of distal force measurement techniques and the second phase focuses on the design improvement to meet the requirements. The tele-operation requirement is met by designing the robotic system as two units: a sensing unit and a robot unit. The sensing unit is the master controller and the robot unit is the slave manipulator. To eliminate the demand on surgeon to learn new skills to operate the controller, the conventional natural hand actions as shown in Fig. 10 are captured by the sensing unit.

3.2.1 Phase-1 Development

The frames are built with acrylic material. Conventional surgical guidewire is used for testing the device. To effect the translation motion, friction roller mechanism is chosen. A pair of rubber cushioned friction rollers rollers are used in robot unit and a set of plastic rollers are used in sensing unit.

3.2.1.1 Sensing Unit

The sensing unit as shown in Fig. 3.1 consist of a pair of friction rollers, hollow shafts to conduct the surgical tool, slip ring assembly, micro vibration motor and two continuous potentiometers. The two plastic friction rollers are placed at a fixed distance such that the distance between the roller's outer diameter is slightly lesser than guidewire diameter. This ensures constant contact between the roller and guidewire. One of the rollers shaft is coupled to a rotary potentiometer P_1. With this assembly, when the guidewire is advanced or retrieved by the surgeon, the continuous translation motion of the guidewire is captured by the P_1. The tool passes through the annular shafts which are coupled to another potentiometer P_2 which inturn measures the rotation of the shaft. This extension of the shaft is used by surgeons to effect rotation, as the rollers hold the guidewire firmly. The slip-ring facilitates the electrical connection between the potentiometer on the rotating parts to the controller without wire entanglement. The measurement from both the potentiometers are converted into command signal by the controller. These

control signals are send are send to the robot unit to drive the actuators. For the purpose of haptic feedback, the sensing unit is installed with a micro vibration motor which is actuated when the distal force measured exceeds a set limit.

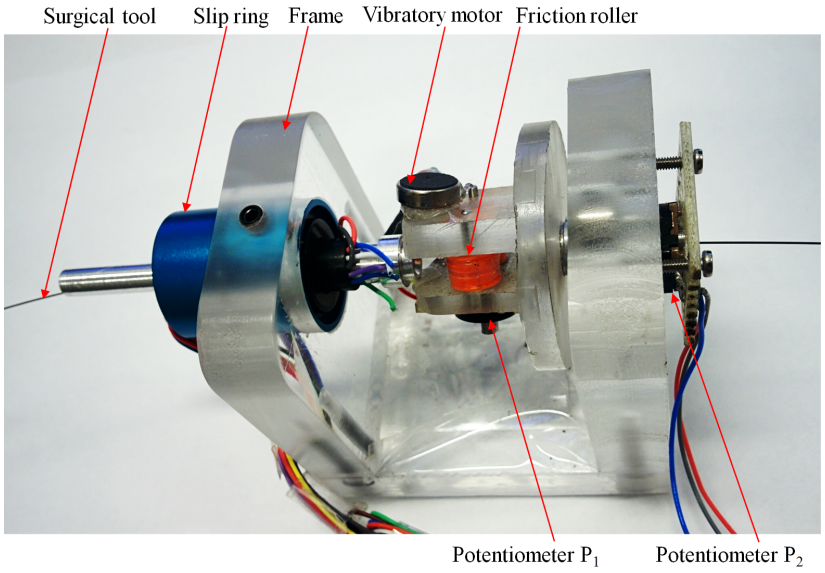

Figure 3.1: Sensing unit phase-1

3.2.1.2 Robot Unit

Construction of robot unit as shown in Fig. 3.2 is similar to sensing unit except that the potentiometers are replaced with motors. A pair of rubber cushioned roller are placed at a fixed distance ensuring constant contact between the guidewire and the rollers. One of the rollers (called active roller) is coupled to a motor m_2 and the other roller(called passive roller) is mounted on a bearing. The rotation of motor m_2, rotates the active rollers and thus the passive roller, which is in contact. The guidewire passing in between these rollers is positively driven because of the frictional contact. Thus the rotation of the rollers results in translation of guidewire. The translation unit is rotated about the axis by another motor m_1 coupled via a gear train. Similar to sensing unit, the slip ring facilitates the continuous electrical and data communication. These actuators are driven by the controllers to replicate the motion captured by sensor unit.

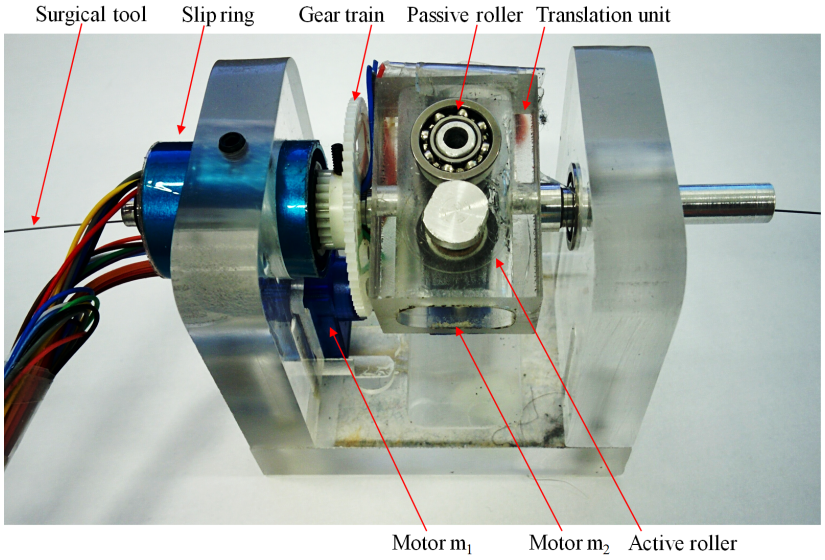

Figure 3.2: Robot unit phase-1

3.2.1.3 Force Sensing Principle

The reaction force experienced by the surgical tool inside the vasculature is transmitted to the distal end. Conventionally, surgeons experience this reactive force on hand due to resultant force from the applied thrusting force (to navigating the guidewire) and the opposing forces on the guidewire. Yang et al [50] used this concept, where the promoting finger on the guidewire feeding robot is equipped with pressure sensors to measure this distal force. Similarly, in the developed robot unit, the driving friction rollers will experience the reaction force. This mechanical load on the actuator is reflected in the current drawn by the actuator to drive the rollers. The current drawn is directly proportional to the torque developed by the motor.

$$\tau = K_t I \tag{3.1}$$

$$F = \tau / R \tag{3.2}$$

where τ is the torque developed by the motor, I is the current drawn by the motor, K_t is the torque constant of the motor and R is the radius of roller. Force applied by the motor is determined from the eqn. 3.2. With

this principle, the resultant force experienced by the motor is determined from the current drawn by the motor using the mathematical relationship as shown above. This force F_s is a sum of two components:

$$F_s = F_n + F_o \tag{3.3}$$

where F_o the nominal force which represents the operating current of the motor for a particular velocity and F_n the reaction force which represents the excess load on the shaft. The nominal force is predetermined from the motor characteristics which could be subtracted from the resultant force to estimate the reaction force.

3.2.1.4 Preliminary Observations

In order to demonstrate the ability to distinguish the actuator operating current and load current while maneuvering the guidewire the following experiment is conducted. To mimic the patient's vasculature, a phantom model is made out of transparent tubes and placed near the robotic device as shown in Fig. 3.3. To measure the actuator current, current sensor was connected in series to the power supply. To observe characteristic of data while manuvering a guidewire in different conditions three different experiments are performed 1. nominal operating condition of actuator, 2. maneuvering straight vasculature section and 3. maneuvering curved vasculature section. In order to observe the operational current of the actuator, the guidewire was maneuvered in an unconstrained conditioned outside phantom and the corresponding current data were stored. In case of maneuvering inside vasculature, the guidewire has to navigate a straight region and a curved region inside the vasculature. A curved section offers more reaction force than straight section because of change in direction. Observing this characteristic behavior in current measurement is essential to distinguish the different loading conditions.

The following observations are made: 1. the actuator operating current is minimal when the there is no resistance offered to the motion of guidewire, 2. The actuator current experienced more load while navigating a curved region compared to a straight region.

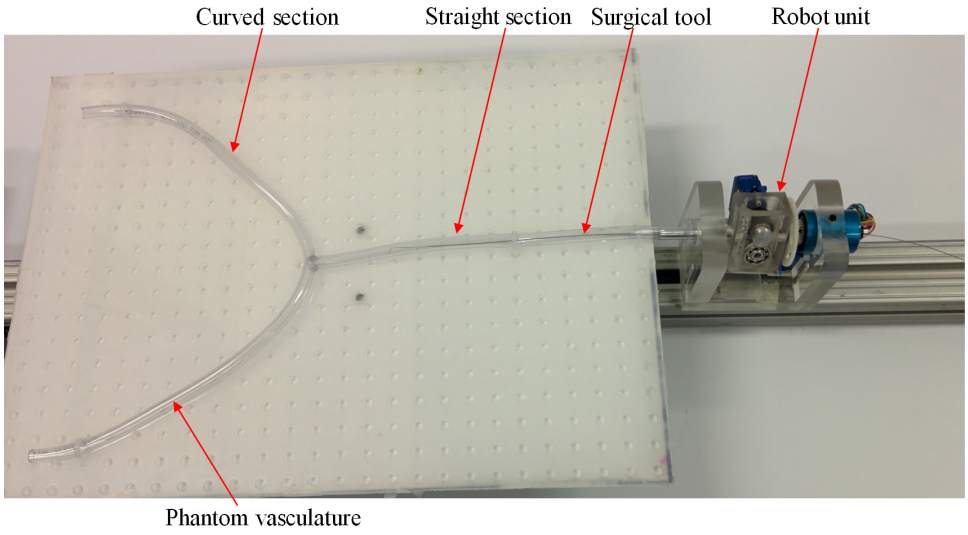

Figure 3.3: Setup distal force verification

3.2.1.5 Results of Phase-1 Prototype

The following are the results phase-1 development:

- The interventional robotic system are built with tele-operation capability facilitating isolation from hazardous radiation.
- The user interface provided with the sensing unit captures surgeon's conventional hand motions without demanding new skill to operate the robot unit.
- A continuous uninterrupted translation motion control of surgical tool are provided with friction roller mechanism.
- Distal force sensing principle from the actuation current is formulated.
- Force measurements are verified with a demonstration in different maneuvering conditions.
- The device performed the maneuvering and sensing with conventional surgical tools eliminate the need for an active catheters.
- Haptic feedback is provided to surgeons upon analyzing the reaction forces to ensure patients' safety.

The following are the issues identified in this phase-1:

- The sensing unit performance were affected due to the use of potentiometer sensor which has low resolution of sensing. In addition physical contacts in potentiometers introduce frictions leading to poor signal to noise ratio.
- Maneuvering of surgical tool were inconsistent due to slipping issues in rubber cushioned friction rollers.
- Since low cost servo motor were used the system parameters like backlash were not consistent and were difficult to quantify. This let to large variation in the current measurements.

3.2.2 Phase-2 Development

The interventional robotic system developed in phase-1 demonstrated the capabilities of a tele-operated robotic system to perform endovascular procedures using conventional guidewire and catheter. The issues identified in the phase-1 development are addressed in the phase-2 development. The sensing unit resolution issue is resolved by using high resolution optical encoders. The slipping issue with the friction rollers is addressed by using knurled roller.

3.2.2.1 Master Console

The master console consists of sensing unit and a display monitor. Surgical tool passes through the sensing unit. Surgeon uses this tool to perform the actions similar to a conventional endovascular procedure. The sensor unit has a pair of knurled rollers. One of the rollers is moveable using a spring-loaded slide to ensure constant gripping force on the tool and the other roller is fixed to which an encoder (E_2) is attached. This adjustable spring-loaded mechanism with quick release plate facilitates the sensing unit to accommodate wide range of surgical tools. These are housed within box unit (BS_1) as shown in the Fig. 3.4. BS_1 is attached to hollow shafts radially aligned with the contact line of the rollers. The shafts are made hollow so that the tools can pass between the rollers. In order to effect the twisting action using a torquer, the surgeon rotates torqueing shaft. To capture this rotating action another encoder (E_1) is mounted on the shaft. The design of

friction wheel is different from the existing design because our design provides area-contact and hence more friction for a positive drive. The existing design is a lower pair mechanism with only a point-contact between the tool and the friction wheel. This leads to slipping when the surgeons perform actions at a faster rate. Knurled rollers are used which provides area-contact leading to a nonholonomic constraint [56] for slip-free drive. Encoder (E_2) attached to the roller shaft measures the translation of the tool using the nonholonomic velocity relationship which is given by

$$\omega_t = \frac{\triangle e \left(\frac{360}{q}\right) \left(\frac{\pi}{180}\right)}{\frac{\triangle t}{1000}} \tag{3.4}$$

$$v_t = r/\omega_t \tag{3.5}$$

where ω_t is the angular velocity measured by the encoder, $\triangle e$ is the change in encoder value, q is the resolution of the encoder, $\triangle t$ is the change in time in milliseconds, v_t is the translational velocity of the tool and r is the roller radius.

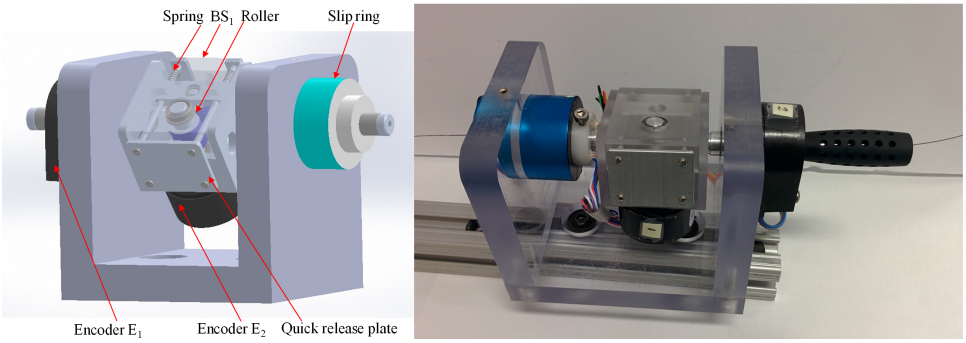

Figure 3.4: Sensing unit phase-2 (left: CAD model, right: Actual model)

Similarly, for steering (rotational motion), a torquer (as shown in Fig. 1.10) is used by the surgeon to twisting the surgical tool. The torquer provides enough grip to twist the surgical tool. In this design similar torquer is provided (torqueing shaft) through which the surgical tool passes. The rotations of the torqueing shaft are captured by encoder (E_1). The encoder measurements are converted to angular velocity, of the surgical tool using the relationship,

$$\dot{\theta} = \omega_r \tag{3.6}$$

where ω_r is the angular velocity measured by the encoder. The torquer in the conventional procedures has a collet that grips the tool. In our design, this gripping is inherently achieved by the knurled rollers [57].

3.2.2.2 Slave Manipulator

Robot unit controls the surgical tool in order to navigate through the vasculature as commanded by the surgeon using the sensor unit. The construction of the robot unit is similar to sensor unit except for the rotary actuators in place of encoders as shown in Fig. 3.5. Similar to BS_1 of sensing unit, robot unit has a box unit BS_2 which houses rollers. The box units are developed with modular design concept to ease disassembling for sterilization. The fixed roller is mounted on the shaft of actuator, m_2, which in turn is attached to BS_2. The moveable roller is on a spring-loaded slide which facilitates surgeons to override the robot to manually move the tool in case of emergency. The unbalanced weight of the motor and other components within $BS2$ are balanced about the axis of BS_2 using a counter-weight. BS_2 is rotated about axis of the shaft by the actuator m_1 coupled through a spur-gear train. Actuation by m_2 effects the translation motion and actuation by m_1 effects the rotation motion of the tool. The control signals to and the encoder data from m_1 is transferred to the controller using a slip-ring similar to the sensor unit.

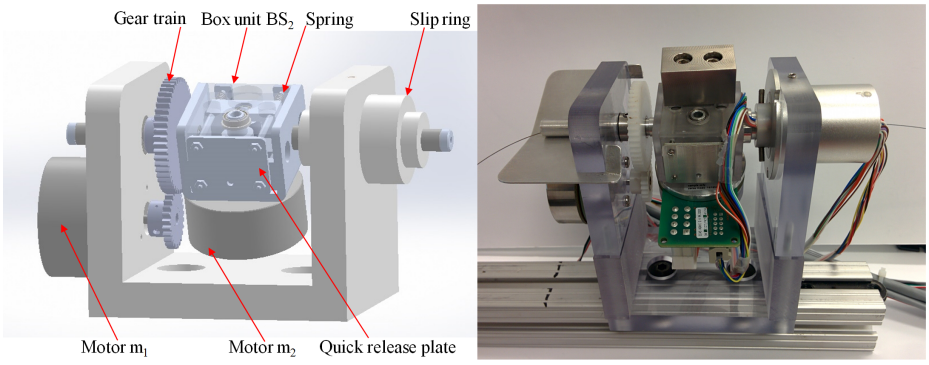

Figure 3.5: Robot unit phase-2 (left: CAD model, right: Actual model)

Our robot has two degrees of freedom(DOF) and two degrees of actuation making this a completely controllable system. The rotational motion of tool is achieved by rotating the BS_2 of mass M by angle θ_{m_1} driven by motor(m_1) with torque τ_{m_1} . The translational motion is achieved by angular rotation θ_{m_2} of the pair of rollers by motor (m_2) with torque τ_{m_2} within the box unit (BS_2). Euler-Lagrange formulation is used to develop the equations of motion (EOM). The potential energy component of the EOM is contributed by unbalanced rotating mass of BS_2 and the torsional stiffness k [58] of the surgical tool. EOM are,

$$J_{m_1}\ddot{\theta}_{m_1} + (C_1 + C_2)\dot{\theta}_{m_1} + Mgl\ \sin\theta_{m_1} + k\theta_{m_1} = \tau_{m_1} - r_t F_t \tag{3.7}$$

$$J_{m_2}\ddot{\theta}_{m_2} + C_3\dot{\theta}_{m_2} = \tau_{m_2} - r_r(\mu F_r + F_t) \tag{3.8}$$

where J_{m_1} is the combined rotational inertia of the box BS_2 and motor m_1, J_{m_2} is the combined rotational inertia of the rollers and the motor m_2. C_1 and C_3 is the damping coefficient of the motor m_1 and m_2 respectively and C_2 is the damping coefficient of slip ring, F_r is the roller spring force, F_t is the friction force at the contact point of tool with tissue, μ is the coefficient of friction on surgical tool surface, l is the length of BS2 from the axis of rotation and r_r and r_t are the radius of friction wheel and radius of the vasculature respectively.

3.3 Control Architecture

The control architecture includes the master sensing unit, slave robot unit and the vasculature environment. The controller design requirements are: 1. surgical tool position tracking and 2. surgeon's action replication and 3. control scheme for safety mechanism. The control architecture as shown in Fig. 3.7 consists of haptic feedback module and a cascade controller module. The haptic feedback module encapsulates all subsystems between surgeon and vasculature. This subsystem gets the surgeons actions $[F, \tau]$ as input and drives the tool inside the vasculature. The force sensed by the robot unit from the vasculature is used to provide haptic feedback to surgeons to ensure

patient's safety. The cascade controller module has the sensing unit and robot unit as subsystems. This module gets the surgical tool motion parameters $[x, \theta]_u$ in sensing unit as inputs and replicates the same using robot unit ensuring the tool position tracking and for surgeon's action replication.

3.3.1 Haptic Feedback Module

When the procedure begins, identical surgical tools are used into the sensing unit and the robot unit. Surgeon applies a force F to perform the translation and a torque τ for rotation of the surgical tool in the sensing unit. These control inputs from surgeon's $[F, \tau]$ result in surgical tool movements as $[x, \theta]_u$ which are captured by the sensing unit and transformed by the rotary sensors as positions $[\theta_1, \theta_2]_d$. The robot unit replicates these captured motions by actuating the motors using commands $f([\theta_1, \theta_2]_a)$. By the virtue of the friction roller design of the robot, actuators responses $[\theta_1, \theta_2]_a$ are transformed to motion $[x, \theta]_g$ of surgical tool. The total force F_n acting on the tool while maneuvering inside the vasculature is reflected in the current drawn by the actuators. The measured current i is converted to force F_s by the impedance relationship Z_h^{-1} as given in eqn. 3.1 and 3.2. This resistive force is monitored continuous by the dead-zone algorithm which triggers whenever the value of resisitve force goes beyond the dead-zone limit. This signal opens a normally closed switch to cease motor actuation providing a safety mechanism. This also triggers the vibratory and audio systems in the sensing unit to alert the surgeons.

3.3.2 Cascade Controller Module

In order to have simultaneous position and velocity controls to track the surgical tool as well as to replicate surgeon's actionss, a cascade controller[59] is used. Abrupt changes in $[\theta_1, \theta_2]_d$ are observed due to three events: 1. rapid movement of user interface, 2. rotating components revolves rapidly for small change in motion and 3. loss of data during communication between controllers and computers. This results in either whipping action of the tool or impulsive thrusting force or damage to the motor due to large current drawn. This undesirable inputs must be modified such that the ve-

locity gradient is small. this modification of input is achieved using shaping [60]. Input shaping is a type of command generation scheme obtained by convolving a sequence of impulses with input signal. In Fig. 3.6, the input signal has a change in magnitude of L which is convoluted with a sequence of impulses $A_1, A_2, ...A_n$ and the corresponding shaped input is shown on the right. this is expressed as

$$y_k(t) = L\sum_{j=1}^{k} A_j \qquad \text{where} \sum_{i=1}^{n} A_i = 1 \tag{3.9}$$

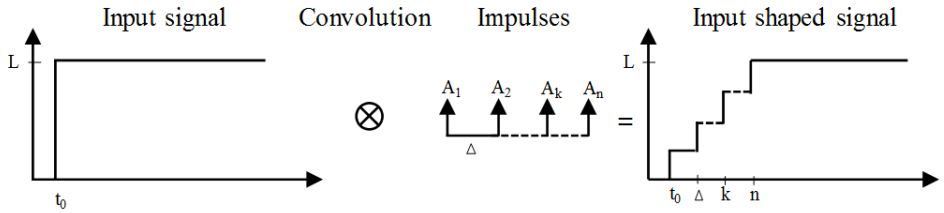

Figure 3.6: Input shaping process

In order replicate surgeon's actions, velocity control is employed. To ensure that commanded position $[\theta_1, \theta_2]_d$ is reached a position control is also used. The two controllers are used is cascade mode in which an error in position is also compensated by the velocity controller. From the control architecture as shown in Fig. 3.7, the position loop is closed using a proportional-integral-derivative(PID) controller and similarly, the velocity loop is closed using another PID controller. The desired position parameter $[\theta_1, \theta_2]_d$ as measured by sensor are constantly compared with the actual position of the robot unit measurements $[\theta_1, \theta_2]_a$. This position error is made as input to the position controller to generate the control inputs that are added to desired velocity. On the other hand, the desired velocities $[\dot{\theta}_1, \dot{\theta}_2]_d$ are provided to control the motor via a normally closed switching unit. The switching unit algorithm acts a safety mechanism to respond to an excessive force measured in the system. It facilitates normal velocity control by default and ceases actuation for safety upon receiving a trigger signal. In case of normal operation, this velocity is provided as input to the PID velocity controller. The control efforts from this controllers is saturated in order to eliminated undesirable output control commands to the motor.

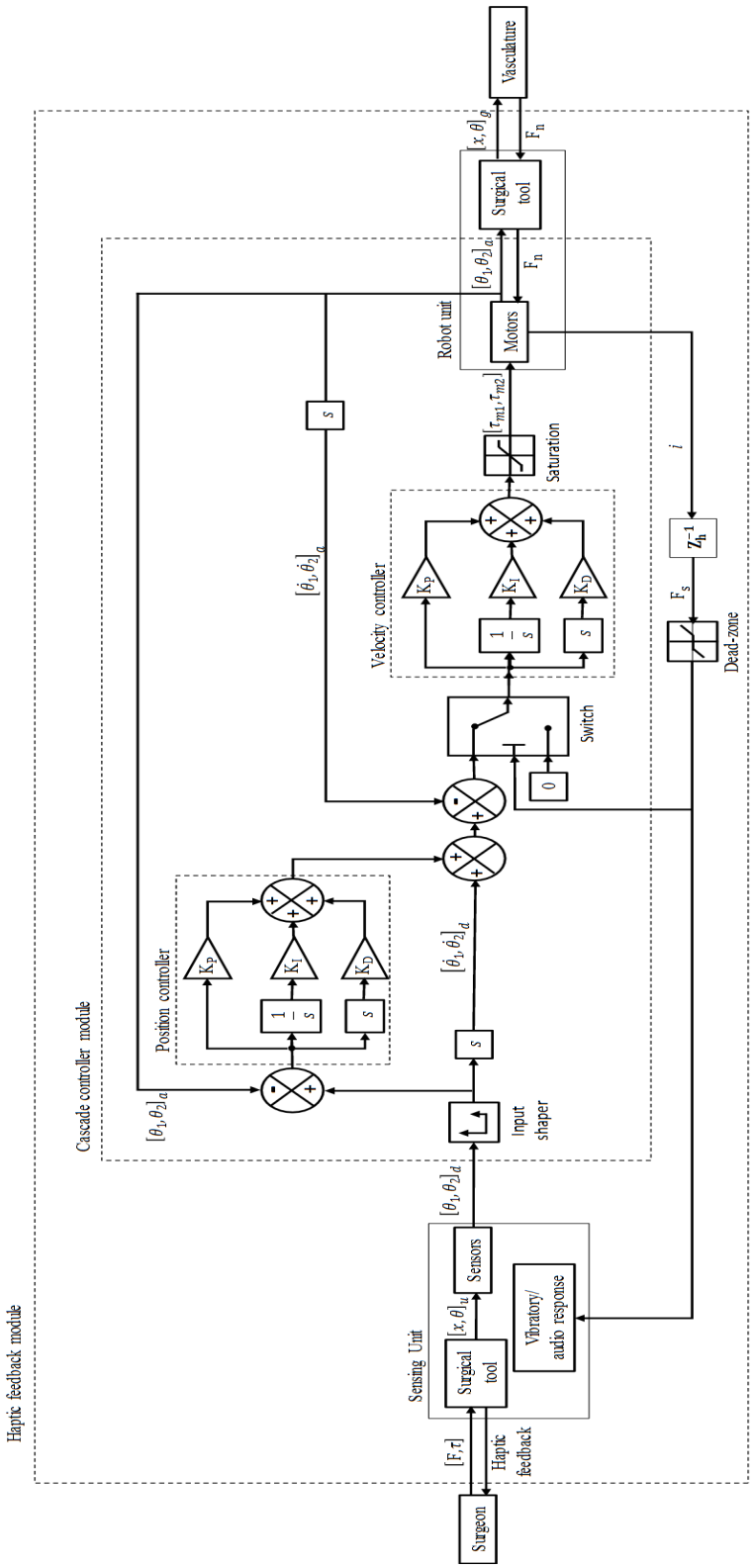

Figure 3.7: Control architecture block diagram

CHAPTER 4

Experimental Validation of Force Measurement

The reaction force experienced by the tool while navigating vasculatures is an essential parameter to aid successful accomplishment of a procedure. The capability to distinguish these forces is demonstrated with the interventional robotic system developed in phase-1 as discussed in chapter 3. In phase-2 IRS, the in-built sensing feature of motor controller allows distal force measurement experienced by the surgical tool. To cross-validate the force computations from robot unit, standard load-cell sensor is used to measure and record these forces simultaneously. This chapter describes the experimental setup, force analysis and results.

4.1 Experimental Setup and Data Collection

The experimental setup as shown in Fig. 4.1 consists of the robot unit, a standard load cell(Phidgets Micro Load cell # 3133) and guidewire as surgical tool. The robot unit and the load cell sensor are mounted on a platform such that the motion of the guidewire is opposed by the load cell. The translational motion of the guidewire driven by actuator experiences the resistive force from the vasculature. The motor experiences this force as load against the desired motion commanded by the controller. To overcome this excessive load in the system the motor draws additional current more than the nominal operating current to drive the guidewire. The current drawn by the motor is measured using an in-built sensor in the motor controller. Load cell and current sensor data are recorded simultaneously. After starting the motor from rest, it is operated at a constant velocity of 30 RPM to drive the guidewire without resistive force and once the guidewire comes in contact with the load cell the actuator experience opposing load. The actuator continues to drive the guidewire applying more force on the load

cell.

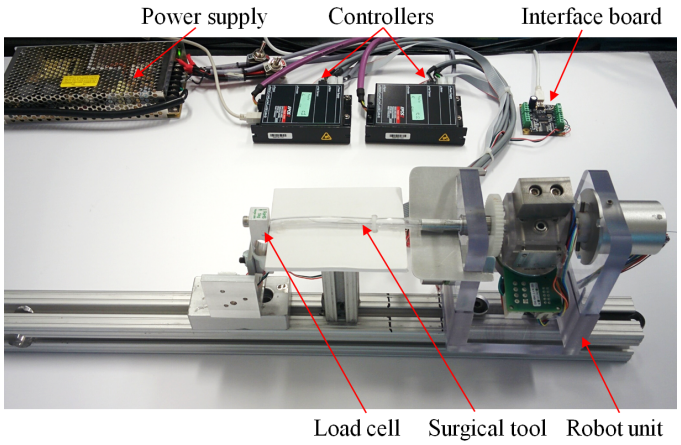

Figure 4.1: Force validation setup

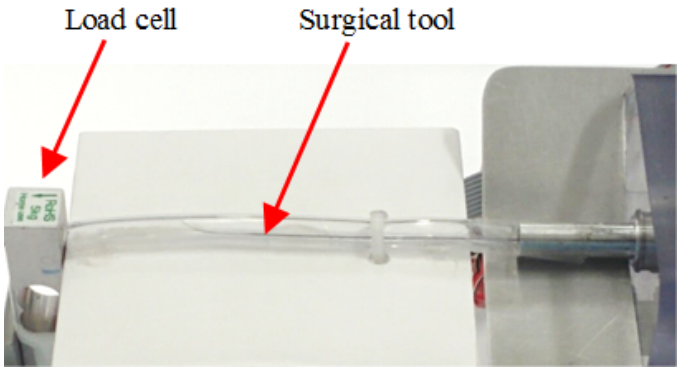

Figure 4.2: Force validation setup: vasculature and load cell

As mentioned in chapter 3, the current drawn by the motor reflects force from the vasculature. The current drawn by the armature contains two components

$$i = i_v + i_n \tag{4.1}$$

where i_n is the nominal operating current of the motor which is a function of motor velocity v which is given by

$$i_n = f(v)$$

and i_v is the current drawn due to reaction force from the vasculature. The total load on motor as a function of i is shown in Fig. 4.3. The blue curve

between 7 to 11s represent load on the motor during nominal operation. The excursion of the curve between 12-16s is due to the reaction load from the vasculature. This is confirmed by the direct load cell measurement as shown by the red curve. Reaction force is a sum of friction and other reaction forces. Since friction cannot be directly measured, only a small section of the phantom vasculature is used in which the friction is negligible. As a result the total load on the motor is the reaction force provided by the load cell.

The measured force data from the load-cell and estimated data from the current are shown in Fig. 4.3. Red line corresponds to the load-cell measurement and the blue line corresponds to the motor force calculated as a function of current. The blue line data represents the net force experienced by the motor. The different sections of the graph (I),(II) and (III) represent the various events of the experiments as described earlier.

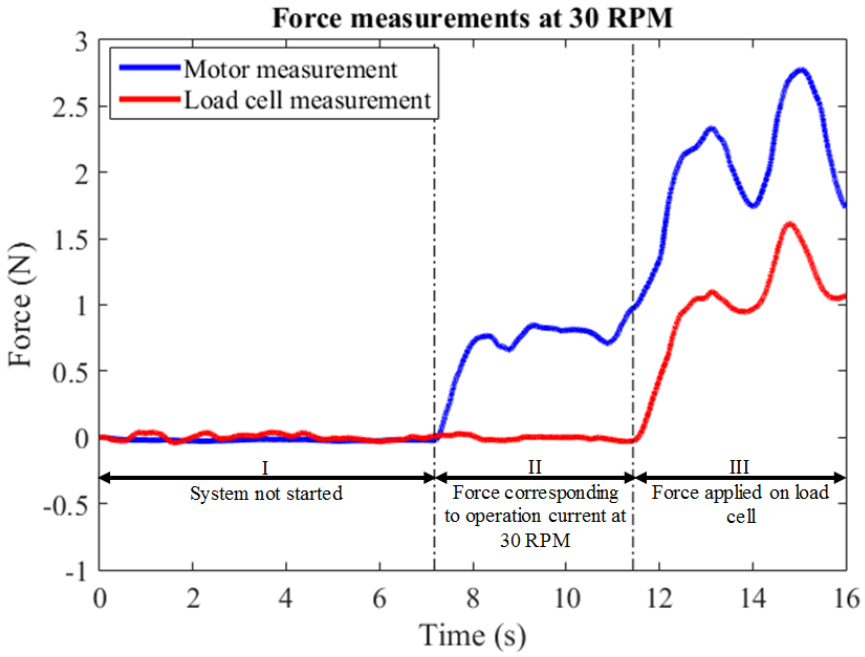

Figure 4.3: Force measurement data

The (I) section of the graph which shows zero force measurement represent the data recorded corresponding to motor at rest. The (II) and (III) sections of the graph represent data corresponding to motor operating constantly at 30 RPM. In the section (II), the tool is advanced inside phantom vasculature section without obstacle and the tool is not in contact with load cell at this stage. The forces observed in this section in motor measurement corresponds

to the normal operating current of motor at 30RPM and zero load is recorded by the load-cell. This bias between the load cell measurement and force estimation is explained in the next section. In the (III) section, the tools is advanced to contact the load-cell as the motor continuous to drive the tool against the load cell. The motor measurements in this section represent combined data corresponding to motor operating current and reaction force from load cell. The load cell measurements corresponds to the force applied by the guidewire. This applied force measurement in the load cell is similarly observed in the motor measurements.

4.2 Bias Estimation

To compute this biasing factor, relationship between the force component corresponding to the motor operating current and velocity needs to be determined. For this, the guidewire is driven by the motor at different velocities without phantom vasculature. The i_n corresponding to the nominal operating current are measured at each velocity and the corresponding forces are calculated and recorded. The data is collected twice for each velocity and the mean values of forces calculated for different rpm are shown in Fig. 4.4

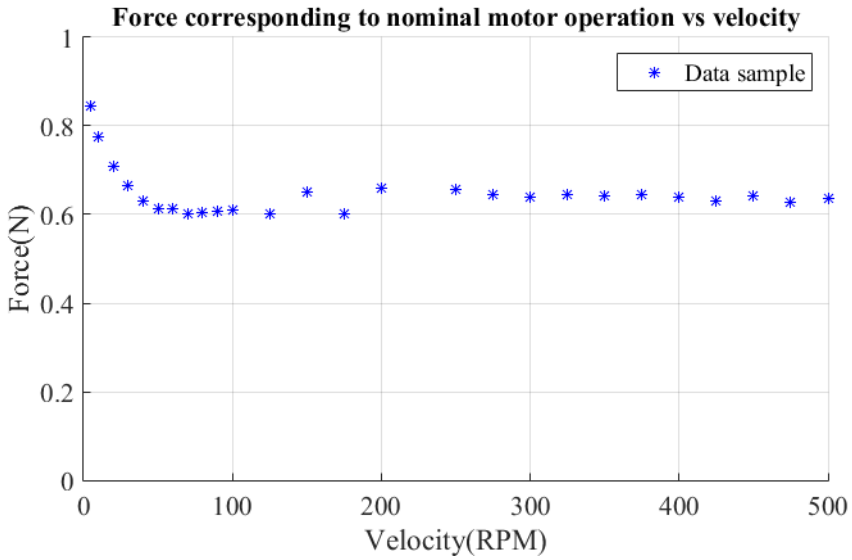

Figure 4.4: Force corresponding to nominal motor operation vs velocity

From the data collected at different values of velocity, different trends are observed for lower range and upper range of velocities as shown in Fig. 4.4.

The lower velocity range has a negative slope and the trend in higher velocity range has a positive slope. Assuming a separation point x_p, for these ranges, linear regression for each of the ranges are given by

For low velocity range v from 0.1 to x_p rpm

$$F_b = m_1 v + c_1 \tag{4.2}$$

For high velocity range v from x_p to 500 rpm

$$F_b = m_2 v + c_2 \tag{4.3}$$

where F_b is the force developed during normal motor operation, v is the velocity in rpm, m_i is the slope and c_i is the y-intercept. A sample of linear regression fit separated at 40 rpm is shown in Fig. 4.5. The corresponding linear regressions are given by eqn. 4.4 and eqn. 4.5.

For low velocity range v from 0.1 to 40 rpm

$$F_b = -0.0058401 v + 0.84709 \tag{4.4}$$

For high velocity range v from 40 to 500 rpm

$$F_b = 6.933e^{-05} v + 0.61235 \tag{4.5}$$

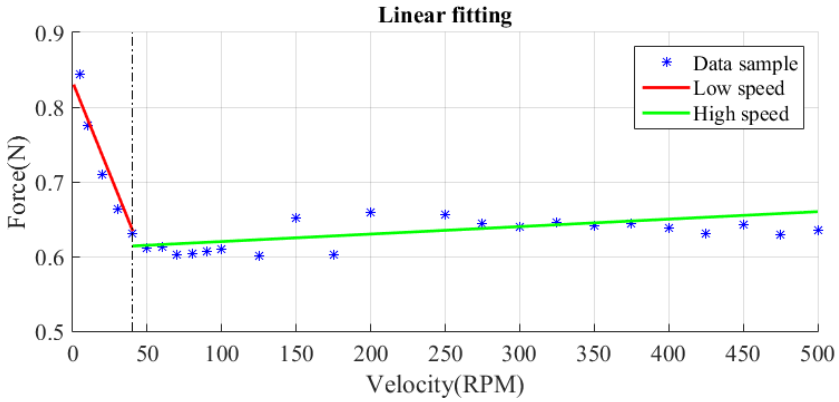

Figure 4.5: Linear fitting

From the graph it is observed that at the separation point x_p both the linear regressions do not represent same nominal force data. The two linear regressions must intersect at the same point at the separation line in-order to

continuously estimate the bias force for all velocity values. This constraint is expressed as

$$x_p\bar{\beta}_1 = x_p\bar{\beta}_2 \qquad \text{where } \bar{\beta}_i = \begin{bmatrix} m_i & c_i \end{bmatrix}^{\mathrm{T}} \tag{4.6}$$

This problem is re-cast as a constrained optimization in which sum of squares of the fitting error is minimized subjected to the constraint given by 4.6. This is given by

$$\begin{aligned} &\min\ e^2 = \frac{1}{2}(\bar{y}_- - \bar{x}_-\bar{\beta}_1)^{\mathrm{T}}(\bar{y}_- - \bar{x}_-\bar{\beta}_1) + \frac{1}{2}(\bar{y}_+ - \bar{x}_+\bar{\beta}_2)^{\mathrm{T}}(\bar{y}_+ - \bar{x}_+\bar{\beta}_2) \\ &\text{subject to} \\ &\qquad x_p\bar{\beta}_1 = x_p\bar{\beta}_2 \qquad \text{where } \bar{\beta}_i = \begin{bmatrix} m_i & c_i \end{bmatrix}^{\mathrm{T}} \end{aligned} \tag{4.7}$$

where e represent discontinuity error between linear regressions, $\bar{x}_-$, $\bar{y}_-$ and $\bar{\beta}_1$ represent the velocity, bias force and parameter respectively corresponding to the data set in the left half of the x_p and similarly $\bar{x}_+$, $\bar{y}_+$ and $\bar{\beta}_2$ represent data set in the right half of the x_p. But the separation point x_p, that separates the two linear regions is not available. This is found out by minimizing the fitting error at two regions given by the optimal solution to the above optimization problem.

The two problems of identifying the optimal separation point x_p and identifying the linear regression models parameters m_1, m_2, c_1, c_2 are together formulated as a bilevel optimization problem [61]. A bilevel optimization, a special class of hierarchical optimization problems, consists of a nested optimization task within the constraint of another optimization problem. The outer optimization is called the upper level task and the inner problem is called lower level task. The nested structure of overall problem requires that a solution to the upper level may be feasible only if it is an optimal solution to the lower level problem. As a result bilevel problems are hard to solve. In this case, the analytical optimal solution to the upper problem is first found, following which the optimal solution to the lower problem is found by searching within the feasible region. This constrained optimization bilevel problem is given by

Upper level problem

$$\min\ e^2 = \frac{1}{2}(\bar{y}_- - \bar{x}_-\bar{\beta}_1)^{\mathrm{T}}(\bar{y}_- - \bar{x}_-\bar{\beta}_1) + \frac{1}{2}(\bar{y}_+ - \bar{x}_+\bar{\beta}_2)^{\mathrm{T}}(\bar{y}_+ - \bar{x}_+\bar{\beta}_2)$$

Lower level problem

subject to

$$\begin{aligned} & x_p \in \underset{x_p}{\operatorname{argmin}} \frac{1}{2}(\bar{y}_- - \bar{x}_-\bar{\beta}_1)^{\mathrm{T}}(\bar{y}_- - \bar{x}_-\bar{\beta}_1) + \frac{1}{2}(\bar{y}_+ - \bar{x}_+\bar{\beta}_2)^{\mathrm{T}}(\bar{y}_+ - \bar{x}_+\bar{\beta}_2) \\ & x_p\bar{\beta}_1 = x_p\bar{\beta}_2 \qquad \text{where } \bar{\beta}_i = \begin{bmatrix} m_i & c_i \end{bmatrix}^{\mathrm{T}} \end{aligned} \tag{4.8}$$

The derivation to this problem is provided in the appendix and the mathematical solution for the upper level problem of identifying the parameter are given by

$$m_1 = \frac{BD_2 + A_2D_1}{A_1A_2 - B^2} \tag{4.9}$$

$$m_2 = \frac{BD_1 + A_1D_2}{A_1A_2 - B^2} \tag{4.10}$$

$$c_1 = c - m_1x_p \tag{4.11}$$

$$c_2 = c - m_2x_p \tag{4.12}$$

where $A_1 = \sum \bar{x}_-^2 - \frac{1}{n}\left(\sum \bar{x}_-\right)^2$, $A_2 = \sum \bar{x}_+^2 - \frac{1}{n}\left(\sum \bar{x}_+\right)^2$, $B = \frac{1}{n}\sum \bar{x}_- \sum \bar{x}_+$, $D_1 = \bar{y}_-^{\mathrm{T}}\bar{x}_- - \mu_{\bar{y}}\sum \bar{x}_-$, $D_2 = \bar{y}_+^{\mathrm{T}}\bar{x}_+ - \mu_{\bar{y}}\sum \bar{x}_+$ and $c = \mu_{\bar{y}} - \frac{m_1}{n}\sum \bar{x}_- - \frac{m_2}{n}\sum \bar{x}_+$

The solution to eqn. 4.9 to eqn. 4.12 is used to find the optimal solution to the lower level problem. The solution is given by quadratic transcendental equation as given below

$$F(x_p) = x_p - g(x_p)^{-1}\left[h(x_p) - f(x_p)x_p^2\right] = 0 \tag{4.13}$$

where

$$f(x_p) = \left(m_1\frac{dm_1}{dx_p} + m_2\frac{dm_2}{dx_p}\right)$$

$$g(x_p) = m_1^2 + m_2^2 + c_1\frac{dm_1}{dx_p} + m_1\frac{dc_1}{dx_p} + c_2\frac{dm_2}{dx_p} + m_2\frac{dc_2}{dx_p} - y_p\left(\frac{dm_1}{dx_p} + \frac{dm_2}{dx_p}\right)$$

$$\begin{aligned} h(x_p) = {} & \sum_{i=1}^{p-1}(y_i - m_1x_i - c_1)\left(\frac{dm_1}{dx_p}x_i + \frac{dc_1}{dx_p}\right) + \sum_{i=p+1}^{n}(y_i - m_2x_i - c_2)\left(\frac{dm_2}{dx_p}x_i + \frac{dc_2}{dx_p}\right) \\ & + y_p\left(\frac{dc_1}{dx_p}x_i + \frac{dc_2}{dx_p} + m_1 + m_2\right) - c_1\left(m_1 + \frac{dc_1}{dx_p}\right) - c_2\left(m_2 + \frac{dc_2}{dx_p}\right) \end{aligned}$$

The numerical methods cannot be used since data for the calculations of parameter m_1, m_2, c_1 and c_2 for intermediate values are not available. Solving quadratic transcendental equation graphically as shown in Fig. 4.6, the solution for the separation point is obtained as $x_p = 41.5586$ and $x_p = 101.8051$. By choosing the nearest values from the collected data, $x_p = 40$ and $x_p = 100$ the associated error is computed as $e_{x_{p=40}} = 0.003471$ and $e_{x_{p=100}} = 0.01684$. Therefore the separation point is $x_p = 40$

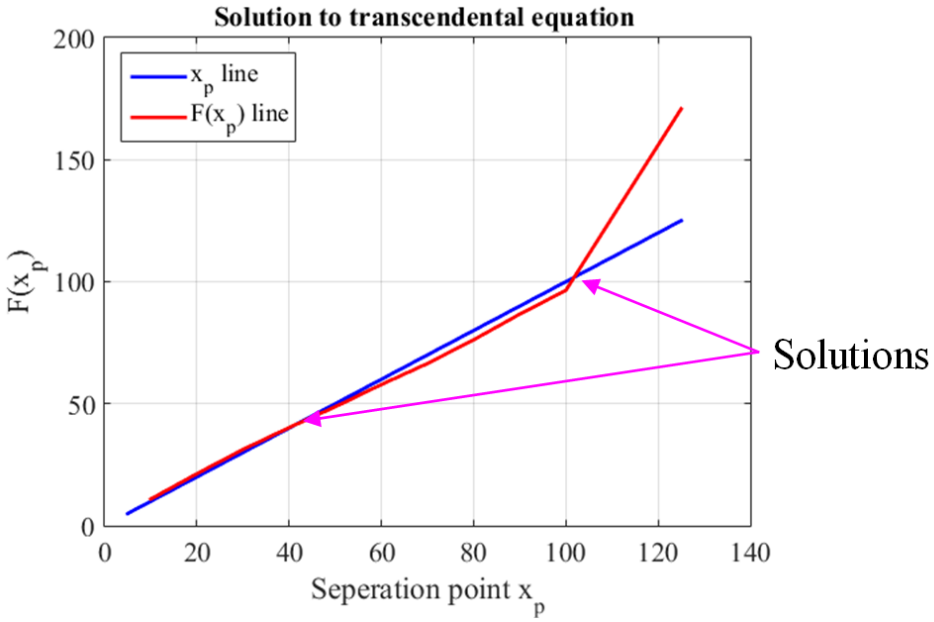

Figure 4.6: Solution to transcendental equation

The parameters m_1, m_2, c_1 and c_2 obtained for the shifted data are used to calculate the intercepts for original data set thus the relationship is given by eqn. 4.14 and eqn. 4.15. Figure 4.7 shows the the data set and the two linear fit relationship.

For low velocity range v from 0.1 to 40 rpm

$$F_b = -0.0059v + 0.8473 \tag{4.14}$$

For high velocity range v from 40 to 500 rpm

$$F_b = 7.5767e^{-05}v + 0.6101 \tag{4.15}$$

Solution to the separation point x_p is confirmed by variation of error as shown in Fig. 4.8. the error is the least at 40 rpm.

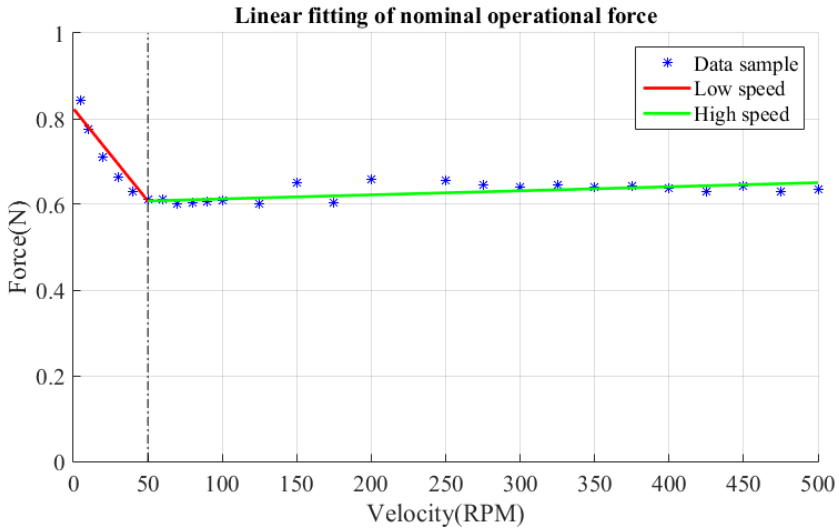

Figure 4.7: Linear fitting of nominal operational force

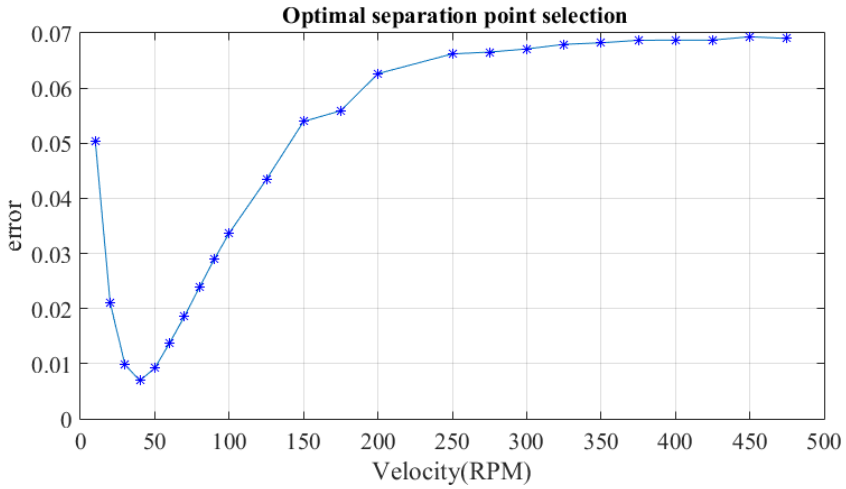

Figure 4.8: Optimal separation point selection

4.3 Validation Results and Summary

The linear regression models expressed in eqn. 4.14 and eqn. 4.15 are used to estimate the bias force F_b for given operation velocity of the motor. The data as shown in Fig. 4.3 is collected by operating the motor at a constant velocity of 30 rpm. Using the linear regression models the corresponding bias force F_b is computed as 0.6716. This bias is applied to the motor force measurement data when the motor starts to operate. The result is shown in Fig. 4.9. The

green line represents the biased force measurement, which is the estimated reaction force sensed by the motor. The load-cell measurement which is the load applied by the guidewire is similarly presented by biased force data.

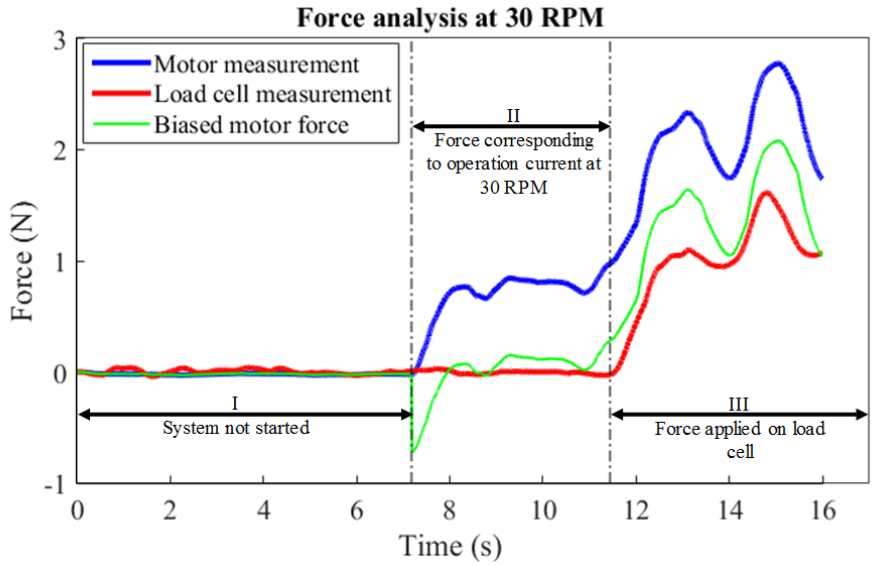

Figure 4.9: Biased force representation

Thus, this linear regression model is used to compute the bias force in real time while navigating guidewire inside vasculature and using this the reaction forces are estimated. As discussed in Chapter 3, this estimated reaction force is continuously monitored to provide haptic feedback to the surgeons.

CHAPTER 5

Performance Evaluation Results

The interventional robotic system developed in phase 2 is evaluated for the following: tele operations, position tracking of surgical tool motion and haptic feedback safety system with force measurement. The setup is shown in Fig. 5.1. The system consists of master console and slave manipulator which are independently mounted with identical guidewires. The master console consists of a display monitor, sensing unit and the surgical tool. The slave manipulator consists of robot unit, controllers, computer, and the surgical tool. Phantom vasculature is used to mimic patient vasculature and a high definition camera is used to mimic the fluoroscopic image of the actual procedure. The master and slave units are isolated as independent modules thus demonstrating the tele-operation capability of the interventional robotic system.

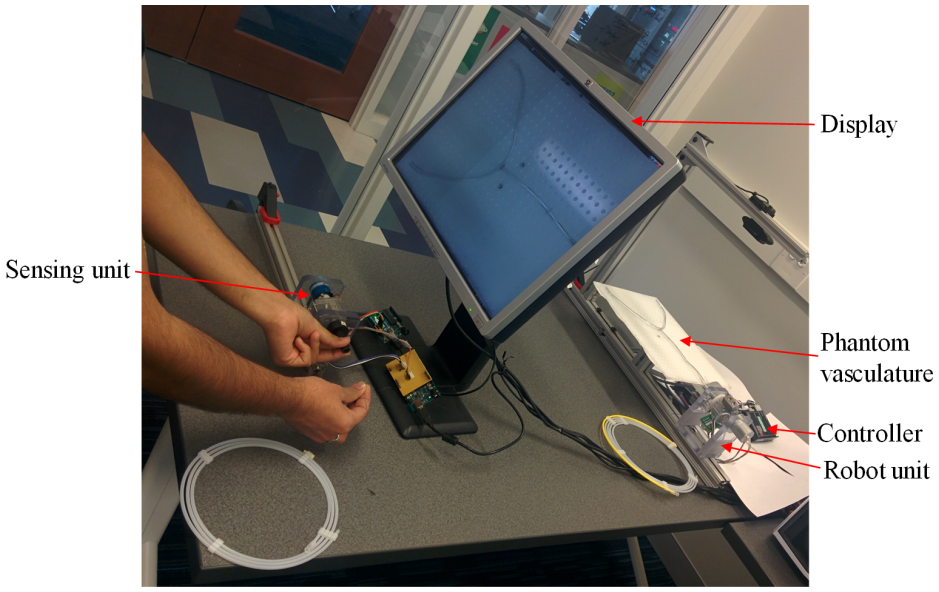

Figure 5.1: Interventional robotic system

5.1 Position Tracking

The developed system has 2 DOF, the control of these motions are independently evaluated by providing actuation from the sensing unit and the observing the corresponding motion of the surgical tool in the robotic unit. The tool motion captured by sensing unit are recorded along with the corresponding motions of the robot unit.

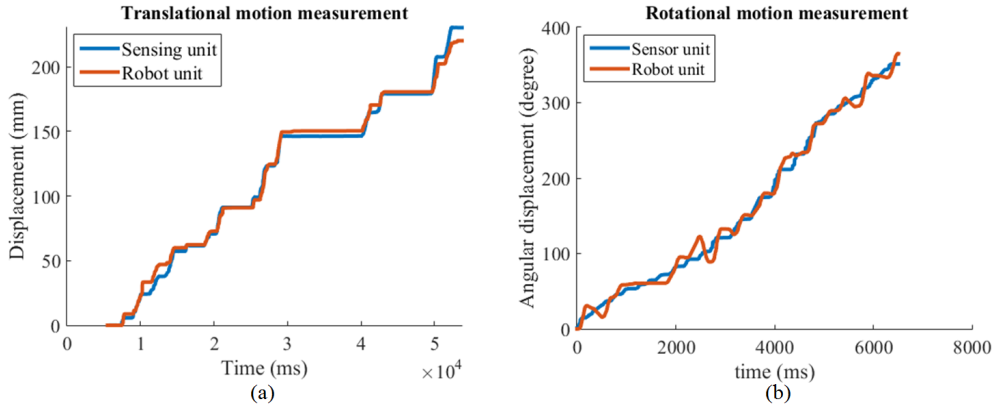

Figure 5.2: (a). Translation motion tracking, (b). Rotational motion tracking

The translational motion data shown in Fig. 5.2(a) and the rotational motion data shown in Fig. 5.2(b) demonstrate the position tracking capability of the slave robotic system. The dynamics system behavior like unbalanced mass and vibration contribute to the undesirable system response from the proportional-integral-derivative(PID) controller.

5.2 Safety Mechanism Based on Force Measurement

The safety mechanism is demonstrated with navigation tasks performed on a branched vasculature as shown in Fig. 5.1 in tele-operative mode. During navigation, the force measurement from the actuators are continuously monitored. Whenever the applied force exceeds this threshold limit as shown in Fig. 5.3, the robot stops advancing the guidewire. In addition, haptic feedback is provided by vibrations to alert the surgeons.

The phantom vasculature as shown in Fig. 5.4, the y-branching of vasculature is close at 140mm. when the reactive force experienced by the guidewire

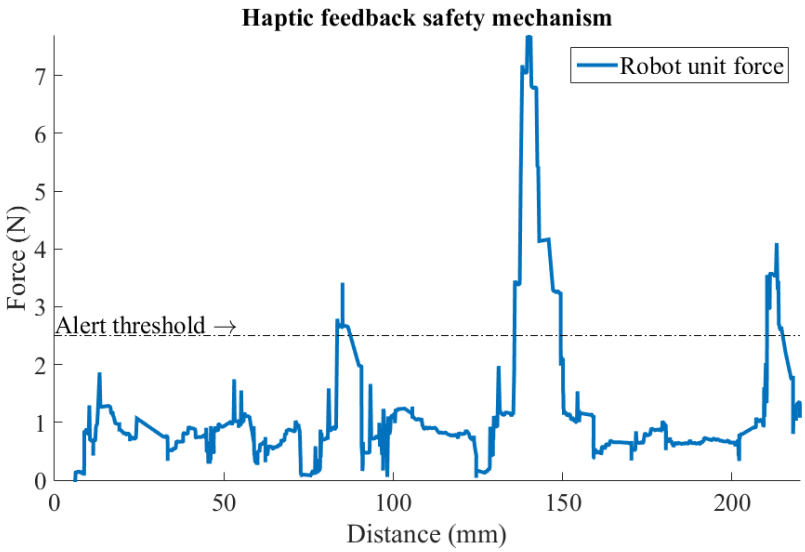

Figure 5.3: Haptic feedback safety system

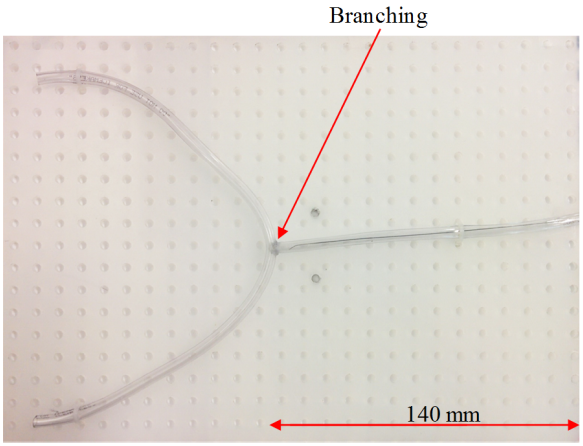

Figure 5.4: Phantom vasculature: Y-Branching

exceeds threshold force of 2.5N (set based on multiple observation) haptic vibration were observed at the master console alerting the user.

CHAPTER 6

Conclusion

The developed of a interventional robotic system that can augment surgeon's administration is successfully developed and demonstrated. The novel user interface of the system operates with conventional surgeon's gestures from a remote console eliminates the need to learn new skill for surgeons. The modular design of robotic unit enable ease system assembly and sterilization.

The device has demonstrated its capability as a safety mechanism in the events of excessive reaction forces while interacting with vasculature. The reaction force estimations are validated with the load cell measurements. Constrained linear regression models are derived to compute the bias force.

A control system developed ensures the function of safety mechanism, haptic feedback, surgical tool position tracking and surgeon's action replication. The performance of the cascade controller for position tracking of surgical tool unit are confirmed with experiments. The performance of passive force estimation in interventional robotic system is verified with real-time haptic feedback during the known occurrences while navigating phantom vasculature. This has eliminated the need for expensive active surgical tools for endovascular robotic procedure.

Future work will provide dexterity with articulated arm for ease of mounting and orienting near patients during procedure. A thorough assessment of issues and impact of robotic assistance in endovascular procedures has to be carried out before a complete in shift in procedures take place.

REFERENCES

[1] Siemens, "Magnetic resonance imaging device, www.usa.healthcare.siemens.com/medical-imaging," 2016,accessed May 30, 2016. [Online]. Available: www.usa.healthcare.siemens.com /medical-imaging

[2] Toshiba, "Computed tomography, www.toshiba.com /resources/img /products/angiography/technology," 2016,accessed May 30, 2016. [Online]. Available: www.toshiba.com /resources/img/products/angiography/technology

[3] Philips, "X-ray, www.usa.philips.com," 2016,accessed May 30, 2016. [Online]. Available: www.usa.philips.com

[4] Robot Application, "Puma 560, www.mogi.bme.hu /tamop/robot-applications/images/image-231.png," 2016,accessed May 30, 2016. [Online]. Available: www.mogi.bme.hu/TAMOP/robot-applications/images/image-231.png

[5] Thinksurgical, "Robodoc hip-replacement surgery, www.thinksurgical.com," 2016,accessed May 30, 2016. [Online]. Available: www.thinksurgical.com

[6] Intuitive surgical, "Da vinci surgical system, www.intuitivesurgical.com," 2016,accessed May 30, 2016. [Online]. Available: www.intuitivesurgical.com

[7] All about Robotic Surgery, "Zeus robotic surgical systems, allaboutroboticsurgery.com /surgicalrobots.html," 2016,accessed May 30, 2016. [Online]. Available: allaboutroboticsurgery.com /surgical-robots.html

[8] Stryker, "Mako robotic-arm assisted surgery, www.stryker.com /en-us/products/orthopaedics/makorobotic-armassistedsurgery," 2016,accessed May 30, 2016. [Online]. Available: www.stryker.com/en-us/products/Orthopaedics/MakoRobotic-ArmAssistedSurgery

[9] NeuroArm, "Neuroarm, www.neuroarm.org," 2016,accessed May 30, 2016. [Online]. Available: www.neuroarm.org

[10] Womens health advice, "Blood clot, www.womens-health-advice.com /assets/images/embolism.jpg," 2016,accessed May 30, 2016. [Online]. Available: www.womens-health-advice.com /assets/images/embolism.jpg

[11] URMC Rochester, "Plaque, www.urmc.rochester.edu /encyclopedia /getimage.aspx?imageid=318796," 2016,accessed May 30, 2016. [Online]. Available: www.urmc.rochester.edu /Encyclopedia/GetImage.aspx?ImageID=318796

[12] David, "Aneurysms, www.daviddarling.info/images/aneurysms.jpg," 2016,accessed May 30, 2016. [Online]. Available: www.daviddarling.info/images/aneurysms.jpg

[13] Service-med, "Aortic-stenosis, www.service-med.com /wp-content/uploads/aortic-stenosis.jpg," 2016,accessed May 30, 2016. [Online]. Available: www.service-med.com/wp-content/uploads/aortic-stenosis.jpg

[14] Cirse org, "Thrombectomy, www.cirse.org /index.php?pid=1071," 2016,accessed May 30, 2016. [Online]. Available: www.cirse.org/index.php?pid=1071

[15] Melbourneheartcare, "Balloon-stent, www.melbourneheartcare.com.au /wp-content/uploads/2011/07/mel0011-illustration-captions34.jpg," 2016,accessed May 30, 2016. [Online]. Available: www.melbourneheartcare.com.au/wp-content/uploads/2011/07/MEL0011-Illustration-Captions34.jpg

[16] Post-gazette, "Alternate catheter route, www.post-gazette.com /news/health/2011/05/30/catheterization-through-wrist-artery-proves-safe-and-effective/stories/201105300122," 2016,accessed May 25, 2016. [Online]. Available: www.post-gazette.com/news/health/2011/05/30/Catheterization-through-wrist-artery-proves-safe-and-effective/stories/201105300122

[17] Gadelius medical, "Guidewire products, www.gadeliusmedical.com /en/products /catheters/related.html," 2016,accessed May 25, 2016. [Online]. Available: www.gadeliusmedical.com/en/products/Catheters/related.html

[18] Vention medical, "Catheter product with balloons, www.ventionmedical.com /assets/img/catheters1.jpg," 2016,accessed May 25, 2016. [Online]. Available: www.ventionmedical.com/assets/img/catheters1.jpg

[19] Boston Scientific, "Active catheter, www.bostonscientific.com /en-us/products/catheters–diagnostic/blazer-dx-20.html," 2016,accessed May 25, 2016. [Online]. Available: www.bostonscientific.com/en-US/products/catheters–diagnostic/blazer-dx-20.html

[20] St. Jude Medical, "Ablation catheter, www.sustainability.sjm.com /innovation.html," 2016,accessed May 25, 2016. [Online]. Available: www.sustainability.sjm.com/innovation.html

[21] Cardiovascular health specialits, "Cardiac catheterization, www.cardiohealthspecialists.com /conditions-treatment/cardiac-catheterization.aspx," 2016,accessed January 8, 2016. [Online]. Available: www.cardiohealthspecialists.com/conditions-treatment/cardiac-catheterization.aspx

[22] P. Schneider, *Endovascular Skills: Guidewire and Catheter Skills for Endovascular Surgery, Informa Healthcare.* CRC Press, Boca Raton, FL, 2008.

[23] Hnamedical, "Torquer, www.hnamedical.com/product," 2016,accessed June 11, 2016. [Online]. Available: www.hnamedical.com/product

[24] Radiologykey, "Aortic arch guidewire navigation, www.radiologykey.com /wp-content/uploads/2016/01/b9781437717198000189-f09-01-9781437717198.jpg," 2016,accessed June 11, 2016. [Online]. Available: www.radiologykey.com/wp-content/uploads/2016/01/B9781437717198000189-f09-01-9781437717198.jpg

[25] Y. S. Kwoh, J. Hou, E. A. Jonckheere, and S. Hayati, "A robot with improved absolute positioning accuracy for ct guided stereotactic brain surgery," *IEEE Transactions on Biomedical Engineering*, vol. 35, no. 2, pp. 153–160, 1988.

[26] W. L. Bargar, A. Bauer, and M. Börner, "Primary and revision total hip replacement using the robodoc (r) system." *Clinical orthopaedics and related research*, vol. 354, pp. 82–91, 1998.

[27] S. Maeso, M. Reza, J. A. Mayol, J. A. Blasco, M. Guerra, E. Andradas, and M. N. Plana, "Efficacy of the da vinci surgical system in abdominal surgery compared with that of laparoscopy: a systematic review and meta-analysis," *Annals of surgery*, vol. 252, no. 2, pp. 254–262, 2010.

[28] H.-X. Zhou, Y.-H. Guo, X.-F. Yu, S.-Y. Bao, J.-L. Liu, Y. Zhang, Y.-G. Ren, and Q. Zheng, "Clinical characteristics of remote zeus robot-assisted laparoscopic cholecystectomy: a report of 40 cases," *World journal of gastroenterology: WJG*, vol. 12, no. 16, p. 2606, 2006.

[29] A. D. Pearle, P. F. O'Loughlin, and D. O. Kendoff, "Robot-assisted unicompartmental knee arthroplasty," *The Journal of arthroplasty*, vol. 25, no. 2, pp. 230–237, 2010.

[30] P. B. McBeth, D. F. Louw, P. R. Rizun, and G. R. Sutherland, "Robotics in neurosurgery," *The American Journal of Surgery*, vol. 188, no. 4, pp. 68–75, 2004.

[31] Corindus Inc., "Corpath 200 robotic system, www.corindus.com," 2015,accessed December 28, 2015. [Online]. Available: www.corindus.com

[32] Hansen Medical Inc., "Magellan system, www.hansenmedical.com /us/en," 2015,accessed December 28, 2015. [Online]. Available: www.hansenmedical.com/us/en

[33] Medtech Insight, "U.s. markets for interventional peripheral vascular disease management products and technologies, www.medtechinsight.com," 2009,accessed December 24, 2015. [Online]. Available: www.medtechinsight.com

[34] P. Lanzer, *Catheter-based Cardiovascular Interventions: A Knowledge-based Approach*. Springer Science & Business Media, 2012.

[35] F. Lorgat, E. Pudney, H. Van Deventer, and S. Chitsaz, "Robotically controlled ablation for atrial fibrillation: the first real-world experience in africa with the hansen robotic system," *Cardiovascular journal of Africa*, vol. 23, no. 5, p. 274, 2012.

[36] E. M. Khan, W. Frumkin, G. A. Ng, S. Neelagaru, F. M. Abi-Samra, J. Lee, M. Giudici, D. Gohn, R. A. Winkle, J. Sussman et al., "First experience with a novel robotic remote catheter system: Amigo mapping trial," *Journal of Interventional Cardiac Electrophysiology*, vol. 37, no. 2, pp. 121–129, 2013.

[37] G. Weisz, D. C. Metzger, R. P. Caputo, J. A. Delgado, J. J. Marshall, G. W. Vetrovec, M. Reisman, R. Waksman, J. F. Granada, V. Novack et al., "Safety and feasibility of robotic percutaneous coronary intervention: Precise (percutaneous robotically-enhanced coronary intervention) study," *Journal of the American College of Cardiology*, vol. 61, no. 15, pp. 1596–1600, 2013.

[38] N. R. Smilowitz, J. W. Moses, F. A. Sosa, B. Lerman, Y. Qureshi, K. E. Dalton, L. T. Privitera, D. Canone-Weber, V. Singh, M. B. Leon et al., "Robotic-enhanced pci compared to the traditional manual approach." *The Journal of invasive cardiology*, vol. 26, no. 7, pp. 318–321, 2014.

[39] P. T. Campbell, K. R. Kruse, C. R. Kroll, J. Y. Patterson, and M. J. Esposito, "The impact of precise robotic lesion length measurement on stent length selection: Ramifications for stent savings," *Cardiovascular Revascularization Medicine*, vol. 16, no. 6, pp. 348–350, 2015.

[40] Catheter Robotics Inc., "Amigo remote catheter system, www.catheterrobotics.com," 2016,accessed June 11, 2016. [Online]. Available: www.catheterrobotics.com/CRUS-main.html

[41] Stereotaxis Inc., "Stereotaxis epoch, www.stereotaxis.com," 2016,accessed June 11, 2016. [Online]. Available: www.stereotaxis.com

[42] C. Riga, C. Bicknell, M. Hamady, and N. Cheshire, "Robotically-steerable catheters and their role in the visceral aortic segment." *The Journal of cardiovascular surgery*, vol. 52, no. 3, pp. 353–362, 2011.

[43] G. Nölker, K.-J. Gutleben, B. Muntean, J. Vogt, D. Horstkotte, L. D. Abkenari, F. Akca, and T. Szili-Torok, "Novel robotic catheter manipulation system integrated with remote magnetic navigation for fully remote ablation of atrial tachyarrhythmias: a two-centre evaluation," *Europace*, vol. 14, no. 12, pp. 1715–1718, 2012.

[44] F. Akca, L. Dabiri, and T. Szili-Torok, "Robotic ablation in electrophysiology," in *Cardiac Arrhythmias*. Springer, 2014, pp. 533–541.

[45] L. Di Biase, T. S. Fahmy, D. Patel, R. Bai, K. Civello, O. M. Wazni, M. Kanj, C. S. Elayi, C. K. Ching, M. Khan et al., "Remote magnetic navigation: human experience in pulmonary vein ablation," *Journal of the American College of Cardiology*, vol. 50, no. 9, pp. 868–874, 2007.

[46] N. A. C. Zakaria, T. Komeda, C. Y. Low, M. Makoto, M. Kobayashi, A. Y. Ismail, and R. Dumitrescu, "Development of foolproof catheter guide system based on mechatronic design," *Production Engineering*, vol. 7, no. 1, pp. 81–90, 2013.

[47] J. Guo, S. Guo, L. Shao, P. Wang, and Q. Gao, "Design and performance evaluation of a novel robotic catheter system for vascular interventional surgery," *Microsystem Technologies*, pp. 1–10, 2015.

[48] C. J. Payne, H. Rafii-Tari, and G.-Z. Yang, "A force feedback system for endovascular catheterisation," in *2012 IEEE/RSJ International Conference on Intelligent Robots and Systems*. IEEE, 2012, pp. 1298–1304.

[49] F. Arai, R. Fujimura, T. Fukuda, and M. Negoro, "New catheter driving method using linear stepping mechanism for intravascular neurosurgery," in *Robotics and Automation, 2002. Proceedings. ICRA'02. IEEE International Conference on*, vol. 3. IEEE, 2002, pp. 2944–2949.

[50] X. Yang, H. Wang, L. Sun, and H. Yu, "Operation and force analysis of the guide wire in a minimally invasive vascular interventional surgery robot system," *Chinese Journal of Mechanical Engineering*, vol. 28, no. 2, pp. 249–257, 2015.

[51] G. Srimathveeravalli, T. Kesavadas, and X. Li, "Design and fabrication of a robotic mechanism for remote steering and positioning of interventional devices," *The International Journal of Medical Robotics and Computer Assisted Surgery*, vol. 6, no. 2, pp. 160–170, 2010.

[52] E. Marcelli, L. Cercenelli, and G. Plicchi, "A novel telerobotic system to remotely navigate standard electrophysiology catheters," in *2008 Computers in Cardiology*. IEEE, 2008, pp. 137–140.

[53] M. Tanimoto, F. Arai, T. Fukuda, H. Iwata, K. Itoigawa, Y. Gotoh, M. Hashimoto, and M. Negoro, "Micro force sensor for intravascular neurosurgery," in *Robotics and Automation, 1997. Proceedings., 1997 IEEE International Conference on*, vol. 2. IEEE, 1997, pp. 1561–1566.

[54] P. Polygerinos, D. Zbyszewski, T. Schaeffter, R. Razavi, L. D. Seneviratne, and K. Althoefer, "Mri-compatible fiber-optic force sensors for catheterization procedures," *IEEE Sensors Journal*, vol. 10, no. 10, pp. 1598–1608, 2010.

[55] E. T. Alboliras and Z. M. Hijazi, "Comparison of costs of intracardiac echocardiography and transesophageal echocardiography in monitoring percutaneous device closure of atrial septal defect in children and adults," *The American journal of cardiology*, vol. 94, no. 5, pp. 690–692, 2004.

[56] H. Goldstein, *Classical Mechanics (1950) Cambridge*. Massachusetts.

[57] M. J. Horzewski, "Guidewire torque device for single-hand manipulation," Feb. 28 1995, uS Patent 5,392,778.

[58] J. Schröder, "The mechanical properties of guidewires. part i: Stiffness and torsional strength," *Cardiovascular and interventional radiology*, vol. 16, pp. 43–46, 1993.

[59] P. Karlsson, "Survey of methods of combining velocity profiles with position control," *Marlardalen University, Sweden*.

[60] M. Kenison and W. Singhose, "Concurrent design of input shaping and proportional plus derivative feedback control," *Journal of dynamic systems, measurement, and control*, vol. 124, no. 3, pp. 398–405, 2002.

[61] J. F. Bard, *Practical bilevel optimization: algorithms and applications*. Springer Science & Business Media, 2013, vol. 30.

APPENDIX A

Constrained Optimization Problem for Linear Regression

The solution to this is formulated as constrained optimization problem as follows

Upper level problem

$$\min\ e^2 = \frac{1}{2}(\bar{y}_- - \bar{x}_-\bar{\beta}_1)^{\mathrm{T}}(\bar{y}_- - \bar{x}_-\bar{\beta}_1) + \frac{1}{2}(\bar{y}_+ - \bar{x}_+\bar{\beta}_2)^{\mathrm{T}}(\bar{y}_+ - \bar{x}_+\bar{\beta}_2)$$

Lower level problem

subject to

$$x_p \in \underset{x_p}{\operatorname{argmin}} \frac{1}{2}(\bar{y}_- - \bar{x}_-\bar{\beta}_1)^{\mathrm{T}}(\bar{y}_- - \bar{x}_-\bar{\beta}_1) + \frac{1}{2}(\bar{y}_+ - \bar{x}_+\bar{\beta}_2)^{\mathrm{T}}(\bar{y}_+ - \bar{x}_+\bar{\beta}_2)$$

$$x_p\bar{\beta}_1 = x_p\bar{\beta}_2 \qquad \text{where } \bar{\beta}_i = \begin{bmatrix} m_i & c_i \end{bmatrix}^{\mathrm{T}} \tag{A.1}$$

where $\bar{x}_-$, $\bar{y}_-$ and $\bar{\beta}_1$ represent the velocity, bias force and parameter respectively corresponding to the data set in the left half of the plane and similarly $\bar{x}_+$, $\bar{y}_+$ and $\bar{\beta}_2$ represent data set in the right half of the plane.

$$c_1 = c_2 = c \tag{A.2}$$

therefore, the upper level optimization problem modified as,

$$\min_e \frac{1}{2}(\bar{y_-^{\mathrm{T}}}\bar{y_-} - 2\bar{y_-^{\mathrm{T}}}\bar{x_-}\bar{\beta}_1 + (\bar{x_-}\bar{\beta}_1)^{\mathrm{T}}\bar{x_-}\bar{\beta}_1 + \bar{y}_+^{\mathrm{T}}\bar{y}_+ - 2\bar{y_+^{\mathrm{T}}}\bar{x_+}\bar{\beta}_2 + (\bar{x_+}\bar{\beta}_2)^{\mathrm{T}}\bar{x_+}\bar{\beta}_2)$$

$$\text{subject to} \quad x_p \begin{bmatrix} 0_- & 1 \end{bmatrix} \begin{bmatrix} m_1 & c \end{bmatrix}^{\mathrm{T}} = \begin{bmatrix} 0_+ & 1 \end{bmatrix} \begin{bmatrix} m_2 & c \end{bmatrix}^{\mathrm{T}} \tag{A.3}$$

$$\implies \min_e \frac{1}{2}\Bigg(\bar{y_-}^{\mathrm{T}}\bar{y_-} - 2\bar{y_-}^{\mathrm{T}}\begin{bmatrix}\bar{x_-} & \bar{1}\end{bmatrix}\begin{bmatrix}m_1\\ c\end{bmatrix} + \Big(\begin{bmatrix}\bar{x_-} & \bar{1}\end{bmatrix}\begin{bmatrix}m_1\\ c\end{bmatrix}\Big)^{\mathrm{T}}\begin{bmatrix}\bar{x_-} & \bar{1}\end{bmatrix}\begin{bmatrix}m_1\\ c\end{bmatrix} + \bar{y}_+^{\mathrm{T}}\bar{y}_+ - 2\bar{y}_+^{\mathrm{T}}\begin{bmatrix}\bar{x_+} & \bar{1}\end{bmatrix}\begin{bmatrix}m_2\\ c\end{bmatrix} + \Big(\begin{bmatrix}\bar{x_+} & \bar{1}\end{bmatrix}\begin{bmatrix}m_2\\ c\end{bmatrix}\Big)^{\mathrm{T}}\begin{bmatrix}\bar{x_-} & \bar{1}\end{bmatrix}\begin{bmatrix}m_2\\ c\end{bmatrix}\Bigg) \tag{A.4}$$

$$\implies \min_e \frac{1}{2}\Big(\bar{y_-}^{\mathrm{T}}\bar{y_-} - 2\bar{y_-}^{\mathrm{T}}(\bar{x_-}m_1 + \bar{c}) + (\bar{x_-}m_1 + \bar{c})^{\mathrm{T}}(\bar{x_-}m_1 + \bar{c}) + \bar{y}_+^{\mathrm{T}}\bar{y}_+ - 2\bar{y}_+^{\mathrm{T}}(\bar{x_+}m_2 + \bar{c}) + (\bar{x_+}m_2 + \bar{c})^{\mathrm{T}}(\bar{x_+}m_2 + \bar{c})\Big) \tag{A.5}$$

$$\implies \min_e \frac{1}{2}\Big(\bar{y_-}^{\mathrm{T}}\bar{y_-} - 2\bar{y_-}^{\mathrm{T}}\bar{x_-}m_1 - 2\bar{y_-}^{\mathrm{T}}\bar{c} + m_1^2\bar{x}_-^{\mathrm{T}}\bar{x_-} + 2m_1\bar{x}_-^{\mathrm{T}}\bar{c} + n_1c^2 + \bar{y}_+^{\mathrm{T}}\bar{y}_+ - 2\bar{y}_+^{\mathrm{T}}\bar{x_+}m_2 - 2\bar{y}_+^{\mathrm{T}}\bar{c}) + m_2^2\bar{x}_+^{\mathrm{T}}\bar{x_+} + 2m_1\bar{x}_-^{\mathrm{T}}\bar{c} + n_2c^2 \tag{A.6}$$

differentiating with respect to m_1,m_2 and $\bar{c}$, and equating to zero, we get

$$-\bar{y}_-^{\mathrm{T}}\bar{x_-} + m_1\bar{x}_-^{\mathrm{T}}\bar{x_-} + \bar{x}_-^{\mathrm{T}}\bar{c} = 0 \tag{A.7}$$

$$-\bar{y}_+^{\mathrm{T}}\bar{x_+} + m_1\bar{x}_+^{\mathrm{T}}\bar{x_+} + \bar{x}_+^{\mathrm{T}}\bar{c} = 0 \tag{A.8}$$

$$-\bar{y}_-^{\mathrm{T}}\bar{1} + m_1\bar{x}_-^{\mathrm{T}}\bar{1} + n_1c - \bar{y}_+^{\mathrm{T}}\bar{1} + m_2\bar{x}_+^{\mathrm{T}}\bar{1} + n_2c = 0 \tag{A.9}$$

from eqn. A.9

$$c = \frac{1}{n}\Big(\sum \bar{y} - m_1\sum \bar{x}_- - m_2\sum \bar{x}_+\Big) \tag{A.10}$$

but

$$\frac{1}{n}\sum \bar{y} = \mu_{\bar{y}}$$

$$\implies c = \Big(\mu_{\bar{y}} - \frac{m_1}{n}\sum \bar{x}_- - \frac{m_2}{n}\sum \bar{x}_+\Big) \tag{A.11}$$

therefore,

$$\implies \bar{c} = \Big(\mu_{\bar{y}} - \frac{m_1}{n}\sum \bar{x}_- - \frac{m_2}{n}\sum \bar{x}_+\Big)\bar{1} \tag{A.12}$$

substituting A.12 in A.7 and A.8

$$-\bar{y}_-^{\mathrm{T}}\bar{x_-} + m_1\sum \bar{x}_-^2 + \sum \bar{x_-}\Big(\mu_{\bar{y}} - \frac{m_1}{n}\sum \bar{x}_- - \frac{m_2}{n}\sum \bar{x}_+\Big) = 0 \tag{A.13}$$

$$-\bar{y}_+^{\mathrm{T}}\bar{x_+} + m_2 \sum \bar{x}_+^2 + \sum \bar{x_+}\left(\mu_{\bar{y}} - \frac{m_1}{n}\sum \bar{x}_- - \frac{m_2}{n}\sum \bar{x}_+\right) = 0 \quad \text{(A.14)}$$

rearranging the terms,

$$-\bar{y}_-^{\mathrm{T}}\bar{x_-} + m_1\left(\sum \bar{x}_-^2 - \frac{1}{n}\big(\sum \bar{x_-}\big)^2\right) + \mu_{\bar{y}}\sum \bar{x}_- - \frac{m_2}{n}\sum \bar{x}_- \sum \bar{x}_+ = 0 \quad \text{(A.15)}$$

$$-\bar{y}_+^{\mathrm{T}}\bar{x_+} + m_2\left(\sum \bar{x}_+^2 - \frac{1}{n}\big(\sum \bar{x_+}\big)^2\right) + \mu_{\bar{y}}\sum \bar{x}_+ - \frac{m_1}{n}\sum \bar{x}_+ \sum \bar{x}_- = 0 \quad \text{(A.16)}$$

$$\implies m_1\left(\sum \bar{x}_-^2 - \frac{1}{n}\big(\sum \bar{x_-}\big)^2\right) - \frac{m_2}{n}\sum \bar{x}_- \sum \bar{x}_+ = \bar{y}_-^{\mathrm{T}}\bar{x_-} - \mu_{\bar{y}}\sum \bar{x}_- \quad \text{(A.17)}$$

$$\implies m_1\left(\sum \bar{x}_+^2 - \frac{1}{n}\big(\sum \bar{x_+}\big)^2\right) - \frac{m_1}{n}\sum \bar{x}_+ \sum \bar{x}_- = \bar{y}_+^{\mathrm{T}}\bar{x_+} - \mu_{\bar{y}}\sum \bar{x}_+ \quad \text{(A.18)}$$

let $A_1 = \sum \bar{x}_-^2 - \frac{1}{n}\big(\sum \bar{x}_-\big)^2$, $A_2 = \sum \bar{x}_+^2 - \frac{1}{n}\big(\sum \bar{x}_+\big)^2$, $B = \frac{1}{n}\sum \bar{x}_- \sum \bar{x}_+$, $D_1 = \bar{y}_-^{\mathrm{T}}\bar{x}_- - \mu_{\bar{y}}\sum \bar{x}_-$, $D_2 = \bar{y}_+^{\mathrm{T}}\bar{x}_+ - \mu_{\bar{y}}\sum \bar{x}_+$

$$\implies A_1 m_1 - B m_2 = D_1 \quad \text{(A.19)}$$

$$\implies A_2 m_2 - B m_1 = D_2 \quad \text{(A.20)}$$

solving A.19 and A.20 for the m_1 and m_2, we get

$$m_1 = \frac{BD_2 + A_2 D_1}{A_1 A_2 - B^2} \quad \text{(A.21)}$$

$$m_2 = \frac{BD_1 + A_1 D_2}{A_1 A_2 - B^2} \quad \text{(A.22)}$$

$$c_1 = c - m_1 x_p \quad \text{(A.23)}$$

$$c_2 = c - m_2 x_p \quad \text{(A.24)}$$

This is the solution to the upper level optimization problem. These parameter $m_1, m_2, c_1 and c_2$ obtained for the shifted data are used to calculate the intercepts for data set thus the relationship is given by A.25 and A.26.

For low velocity range v from 0.1 to x_p rpm

$$F_b = m_1 v + C_1 \quad \text{(A.25)}$$

For high velocity range v from x_p to 500 rpm

$$F_b = m_2 v + C_2 \tag{A.26}$$

The lower level problem is rewritten as

$$\underset{x_p}{\operatorname{argmin}} \frac{1}{2}(\bar{y}_- - \bar{x}_- \bar{\beta}_1)^{\mathrm{T}}(\bar{y}_- - \bar{x}_- \bar{\beta}_1) + \frac{1}{2}(\bar{y}_+ - \bar{x}_+ \bar{\beta}_2)^{\mathrm{T}}(\bar{y}_+ - \bar{x}_+ \bar{\beta}_2) \tag{A.27}$$

$$\underset{x_p}{\operatorname{argmin}} \frac{1}{2}\sum_{i=1}^{p}(y_- - m_1 x_- - c_1)^2 + \frac{1}{2}\sum_{i=p+1}^{n}(y_+ - m_2 x_+ - c_2)^2 \tag{A.28}$$

Differentiating A.28 w.r.to, x_p and equating to zero,

$$\begin{aligned}
&\sum_{i=1}^{p-1}(y_i - m_1 x_i - c_1)\left(-\frac{dm_1}{dx_p}x_i - \frac{dc_1}{dx_p}\right) \\
&\qquad + (y_p - m_1 x_p - c_1)\left(-\frac{dm_1}{dx_p}x_p - m_1 - \frac{dc_1}{dx_p}\right) \\
&\qquad + (y_p - m_2 x_p - c_2)\left(-\frac{dm_2}{dx_p}x_p - m_2 - \frac{dc_2}{dx_p}\right) \\
&\qquad + \sum_{i=p+1}^{n}(y_i - m_2 x_i - c_2)\left(-\frac{dm_2}{dx_p}x_i - \frac{dc_2}{dx_p}\right) = 0
\end{aligned} \tag{A.29}$$

$$\begin{aligned}
\implies &\sum_{i=1}^{p-1}(y_i - m_1 x_i - c_1)\left(-\frac{dm_1}{dx_p}x_i - \frac{dc_1}{dx_p}\right) \\
&\qquad + (y_p - m_1 x_p - c_1)(-m_1) \\
&\qquad + (y_p - m_2 x_p - c_2)(-m_2) \\
&\qquad + \sum_{i=p+1}^{n}(y_i - m_2 x_i - c_2)\left(-\frac{dm_2}{dx_p}x_i - \frac{dc_2}{dx_p}\right) = 0
\end{aligned} \tag{A.30}$$

$$
\begin{aligned}
\implies & -\sum_{i=1}^{p-1}(y_i - m_1x_i - c_1)\left(\frac{dm_1}{dx_p}x_i + \frac{dc_1}{dx_p}\right) \\
& \quad - (y_p - m_1x_p - c_1)\left(\frac{dm_1}{dx_p}x_i + \frac{dc_1}{dx_p}\right) \\
& \quad - y_p(m_1 + m_2) + x_p(m_1^2 + m_2^2) + c_1m_1 + c_2m_2 \\
& \quad - (y_p - m_2x_p - c_2)\left(-\frac{dm_2}{dx_p}x_i - \frac{dc_2}{dx_p}\right) \\
& \quad - \sum_{i=p+1}^{n}(y_i - m_2x_i - c_2)\left(-\frac{dm_2}{dx_p}x_i - \frac{dc_2}{dx_p}\right) = 0
\end{aligned} \tag{A.31}
$$

$$
\begin{aligned}
\implies & -y_p\frac{dm_1}{dx_p}x_p + m_1\frac{dm_1}{dx_p}x_p^2 + c_1\frac{dm_1}{dx_p}x_p - y_p\frac{dc_1}{dx_p} + m_1\frac{dc_1}{dx_p}x_p + c_1\frac{dc_1}{dx_p} \\
& - y_p(m_1 + m_2) + x_p(m_1^2 + m_2^2) + c_1m_1 + c_2m_2 \\
& - y_p\frac{dm_2}{dx_p}x_p + m_2\frac{dm_2}{dx_p}x_p^2 + c_2\frac{dm_2}{dx_p}x_p - y_p\frac{dc_2}{dx_p} + m_1\frac{dc_2}{dx_p}x_p + c_2\frac{dc_2}{dx_p} \\
& = \sum_{i=1}^{p-1}(y_i - m_1x_i - c_1)\left(\frac{dm_1}{dx_p}x_i + \frac{dc_1}{dx_p}\right) \\
& + \sum_{i=p+1}^{n}(y_i - m_2x_i - c_2)\left(\frac{dm_2}{dx_p}x_i + \frac{dc_2}{dx_p}\right)
\end{aligned} \tag{A.32}
$$

$$
\begin{aligned}
\implies & \left(m_1\frac{dm_1}{dx_p} + m_2\frac{dm_2}{dx_p}\right)x_p^2 \\
& + \left[m_1^2 + m_2^2 + c_1\frac{dm_1}{dx_p} + m_1\frac{dc_1}{dx_p} + c_2\frac{dm_2}{dx_p}\right. \\
& \left. + m_2\frac{dc_2}{dx_p} - y_p\left(\frac{dm_1}{dx_p} + \frac{dm_2}{dx_p}\right)h(x_p)\right. \\
& = \sum_{i=1}^{p-1}(y_i - m_1x_i - c_1)\left(\frac{dm_1}{dx_p}x_i + \frac{dc_1}{dx_p}\right) \\
& + \sum_{i=p+1}^{n}(y_i - m_2x_i - c_2)\left(\frac{dm_2}{dx_p}x_i + \frac{dc_2}{dx_p}\right]x_p \\
& + y_p\left(\frac{dc_1}{dx_p}x_i + \frac{dc_2}{dx_p} + m_1 + m_2\right) - c_1\left(m_1 + \frac{dc_1}{dx_p}\right) \\
& - c_2\left(m_2 + \frac{dc_2}{dx_p}\right)
\end{aligned} \tag{A.33}
$$

1. $\frac{dm_1}{dx_p}$ from eqn. A.21 $m_1 = \frac{BD_2+A_2D_1}{A_1A_2-B^2}$ and thus $\frac{dm_1}{dx_p}$ is given by

$$\frac{dm_1}{dx_p} = \tag{A.34}$$

$$\frac{(A_1A_2-B^2)\left(\frac{dB}{dx_p}D_2+B\frac{dD_2}{dx_p}+\frac{dA_2}{dx_p}D_1+A_2\frac{dD_1}{dx_p}\right)-\left(\frac{dA_1}{dx_p}A_2+A_1\frac{dA_2}{dx_p}-2B\frac{dB}{dx_p}\right)(BD_2+A_2D_1)}{(A_1A_2-B^2)^2}$$

2. $\frac{dm_2}{dx_p}$ from eqn. A.22 $m_2 = \frac{BD_1+A_1D_2}{A_1A_2-B^2}$ and thus $\frac{dm_2}{dx_p}$ is given by

$$\frac{dm_2}{dx_p} = \tag{A.35}$$

$$\frac{(A_1A_2-B^2)\left(\frac{dB}{dx_p}D_1+B\frac{dD_1}{dx_p}+\frac{dA_1}{dx_p}D_2+A_1\frac{dD_2}{dx_p}\right)-\left(\frac{dA_1}{dx_p}A_2+A_1\frac{dA_2}{dx_p}-2B\frac{dB}{dx_p}\right)(BD_2+A_2D_1)}{(A_1A_2-B^2)^2}$$

3. $\frac{dc_1}{dx_p}$ from eqn. A.23 $c_1 = c - m_1x_p$

$$\frac{dc_1}{dx_p} = \frac{dc}{dx_p} - \frac{dm_1}{dx_p}x_p - m_1 \tag{A.36}$$

4. $\frac{dc_2}{dx_p}$ from eqn. A.24 $c_2 = c - m_2x_p$

$$\frac{dc_2}{dx_p} = \frac{dc}{dx_p} - \frac{dm_2}{dx_p}x_p - m_2 \tag{A.37}$$

5. $\frac{dc}{dx_p}$ from eqn. A.10

$$c = \frac{1}{n}\left(\sum \bar{y} - m_1\sum \bar{x}_- - m_2\sum \bar{x}_+\right)$$

$$c = \frac{1}{n}\left(\sum \bar{y} - m_1\sum(\bar{x}_{1-p} - x_p) - m_2\sum(\bar{x}_{p-n} - x_p)\right)$$

$$\implies \frac{dc}{dx_p} = \frac{1}{n}\left(n_1m_1 + n_2m_2 - \frac{dm_1}{dx_p}\sum \bar{x}_- - \frac{dm_2}{dx_p}\sum \bar{x}_+\right) \tag{A.38}$$

6. $\frac{dB}{dx_p}$ from above,

$$B = \frac{1}{n}\sum \bar{x}_-\sum \bar{x}_+$$

$$B = \frac{1}{n}\sum(\bar{x}_{1-p} - x_p)\sum(\bar{x}_{p-n} - x_p)$$

$$\implies \frac{dB}{dx_p} = -\frac{1}{n}\left(n_1 \sum \bar{x}_+ + n_2 \sum \bar{x}_-\right) \tag{A.39}$$

7. $\frac{dA_1}{dx_p}$ from above, $A_1 = \sum \bar{x}_-^2 - \frac{1}{n}\left(\sum \bar{x}_-\right)^2$,

$$A_1 = \sum (\bar{x}_{1-p} - x_p)^2 - \frac{1}{n}\left(\sum (\bar{x}_{1-p} - x_p)\right)^2$$

$$\frac{dA_1}{dx_p} = 2n_1 x_p - 2\sum x_{1-p} + \frac{2n_1}{n}\sum (\bar{x}_{1-p} - x_p) \tag{A.40}$$

$$\implies \frac{dA_1}{dx_p} = 2n_1 x_p - 2\sum x_{1-p} + \frac{2}{n}\sum \bar{x}_- \tag{A.41}$$

8. $\frac{dA_2}{dx_p}$ from above, $A_2 = \sum \bar{x}_+^2 - \frac{1}{n}\left(\sum \bar{x}_+\right)^2$,

$$A_2 = \sum (\bar{x}_{p-n} - x_p)^2 - \frac{1}{n}\left(\sum (\bar{x}_{p-n} - x_p)\right)^2$$

$$\implies \frac{dA_2}{dx_p} = 2n_2 x_p - 2\sum x_{p-n} + \frac{2}{n}\sum \bar{x}_+ \tag{A.42}$$

9. $\frac{dD_1}{dx_p}$ from above, $D_1 = \bar{y}_-^{\mathrm{T}} \bar{x}_- - \mu_{\bar{y}} \sum \bar{x}_-$,

$$D_1 = \bar{y}_-^{\mathrm{T}} (x_{1-p} - x_p) - \mu_{\bar{y}} \sum (x_{1-p} - x_p)$$

$$\implies \frac{dD_1}{dx_p} = n_1 \mu_{\bar{y}} - \sum \bar{y}_- \tag{A.43}$$

10. $\frac{dD_1}{dx_p}$ from above, $D_2 = \bar{y}_+^{\mathrm{T}} \bar{x}_+ - \mu_{\bar{y}} \sum \bar{x}_+$

$$D_2 = \bar{y}_+^{\mathrm{T}} (x_{p-n} - x_p) - \mu_{\bar{y}} \sum (x_{p-n} - x_p)$$

$$\implies \frac{dD_2}{dx_p} = n_2 \mu_{\bar{y}} - \sum \bar{y}_+ \tag{A.44}$$

Thus Equation A.33 is of the form

$$f(x_p) x_p^2 + g(x_p) x_p = h(x_p) \tag{A.45}$$

$$\implies F(x_p) = x_p - g(x_p)^{-1}\left[h(x_p) - f(x_p) x_p^2\right] = 0 \tag{A.46}$$

where

$$f(x_p) = \left(m_1 \frac{dm_1}{dx_p} + m_2 \frac{dm_2}{dx_p} \right)$$

$$g(x_p) = m_1^2 + m_2^2 + c_1 \frac{dm_1}{dx_p} + m_1 \frac{dc_1}{dx_p} + c_2 \frac{dm_2}{dx_p} + m_2 \frac{dc_2}{dx_p} - y_p \left(\frac{dm_1}{dx_p} + \frac{dm_2}{dx_p} \right)$$

$$h(x_p) = \sum_{i=1}^{p-1} (y_i - m_1 x_i - c_1) \left(\frac{dm_1}{dx_p} x_i + \frac{dc_1}{dx_p} \right) + \sum_{i=p+1}^{n} (y_i - m_2 x_i - c_2) \left(\frac{dm_2}{dx_p} x_i + \frac{dc_2}{dx_p} \right)$$
$$+ y_p \left(\frac{dc_1}{dx_p} x_i + \frac{dc_2}{dx_p} + m_1 + m_2 \right) - c_1 \left(m_1 + \frac{dc_1}{dx_p} \right) - c_2 \left(m_2 + \frac{dc_2}{dx_p} \right)$$

The solution to transcendental equation is obtained numerically (fixed point iteration, newton-raphson, bisecant genetic algorithm etc.)